

MorphingCircuit: An Integrated Design, Simulation, and Fabrication Workflow for Self-morphing Electronics

GUANYUN WANG, Carnegie Mellon University, USA and Zhejiang University, China

FANG QIN, Carnegie Mellon University, USA

HAOLIN LIU, Carnegie Mellon University, USA

YE TAO, Zhejiang University City College, China

YANG ZHANG, Carnegie Mellon University, USA

YONGJIE JESSICA ZHANG, Carnegie Mellon University, USA

LINING YAO, Carnegie Mellon University, USA

Manufacturing nonplanar electronics often requires the integration of functions and forms through embedding circuit boards into three-dimensional (3D) shapes. While most popular solutions rely on cavities where electronics reside in forms of rigid circuit boards, other alternative approaches leverage 3D printing or layer lamination to create 3D electronics that often require expensive manufacturing processes and materials. Furthermore, many conventional methods are incompatible with complex geometries (e.g., surfaces that twist or have local minima). In response, we introduce MorphingCircuit, an integrated design, simulation, and fabrication workflow that combines electronic functions with forms through four-dimensional (4D) printing, which effectively reduces cost, production time, and e-waste. Specifically, we start by printing a flat substrate and assembling functional electronics on top of it. The flat structure will then self-morph into a preprogrammed 3D shape when triggered by external heating. Overall, our comprehensive 3D electronics fabrication pipeline encompasses the design, simulation, fabrication, and transformation, with which we hope to inspire designers, researchers, and makers to create conformal electronics on complex substrate geometries that were previously difficult or impossible to design or manufacture.

CCS Concepts: • Human-centered computing → Human computer interaction (HCI) • Human-centered computing → Ubiquitous and mobile computing → Ubiquitous and mobile computing systems and tools • Hardware~Printed circuit boards → PCB design and layout

Additional Key Words and Phrases: 3D printing; 4D printing; shape-changing interfaces; 3D electronics; 3D circuits; morphing circuits; 3D PCB.

ACM Reference format:

Guanyun Wang, Fang Qin, Haolin Liu, Ye Tao, Yang Zhang, Yongjie Jessica Zhang, Lining Yao. 2020. MorphingCircuit: An Integrated Design, Simulation, and Fabrication Workflow for Self-morphing Electronics. *Proc. ACM Interact. Mob. Wearable Ubiquitous Technol.* 4, 4, Article 157 (December 2020), 26 pages. <https://doi.org/10.1145/3432232>

Corresponding authors' addresses: Guanyun Wang, Carnegie Mellon University, USA, and Zhejiang University, China, guanyun@zju.edu.cn; Fang Qin, Carnegie Mellon University, USA, fangq@stanford.edu; Haolin Liu, Carnegie Mellon University, USA, haolinl@andrew.cmu.edu; Ye Tao, Zhejiang University City College, China, taoye@zucc.edu.cn; Yang Zhang, Carnegie Mellon University, USA, yang.zhang@cs.cmu.edu; Yongjie Jessica Zhang, Carnegie Mellon University, USA, jessicaz@andrew.cmu.edu; Lining Yao, Carnegie Mellon University, USA, liningy@andrew.cmu.edu.

Permission to make digital or hard copies of all or part of this work for personal or classroom use is granted without fee provided that copies are not made or distributed for profit or commercial advantage and that copies bear this notice and the full citation on the first page. Copyrights for components of this work owned by others than ACM must be honored. Abstracting with credit is permitted. To copy otherwise, or republish, to post on servers or to redistribute to lists, requires prior specific permission and/or a fee. Request permissions from Permissions@acm.org.

Copyright © ACM 2020 2474-9567/2020/12 - ART157 \$15.00
<https://doi.org/10.1145/3432232>

1 INTRODUCTION

Recently we have seen a boom of non-planar surfaces equipped with functional electronics for sensing and display. By attaching electronic components and conductive traces directly to the surface of a product, such 3D conformal electronics [9, 19, 74] enable functionalities that flat, rigid electronics do not have: they can be adapted to open 3D surfaces without either cavities or structures where printed circuit boards (PCBs) are conventionally placed; they can enable sensing (e.g., capacitive touch sensing on a 3D surface [28]) and display (e.g., 3D LED panel [43]) directly on the surface of a product; they also allow the integration of form with rich affordance (e.g., a dome-shaped antenna [2, 23]).

Making 3D conformal electronics often involves both 3D substrate construction and circuit attachment. Based on the order of the two fabrication steps, the state-of-the-art techniques to make 3D conformal electronics can be classified into different categories. To attach circuits after the 3D substrate construction, most techniques require specialized processes, including micro extrusion printing [2, 3], jet-based printing [40], lithography processes [21], transfer printing [37, 46], and laser-based direct structuring [71]. Most of the machines required are rather specialized, and the processes are often tedious and costly. On the other hand, Voxel 8 [1] is a multi-material printer that allows us to print circuits and 3D substrate at the same time. However, the mismatch of the thermal expansion ratio between thermoplastic substrates and conductive inks leads to high failure rate [10]. Lastly, the fabrication process that is the most relevant to our paper is applying circuits on a flat substrate, followed by folding the substrate from 2D to 3D. The folding can happen manually [38] or automatically (i.e., self-assembly [11, 16, 34]). To our knowledge, most of the existing self-folding electronics have an origami style [6, 11, 16, 23, 34, 65]. Rather than having continuous 3D surfaces, they are often made of multiple flat faces connected by folding hinges. While vacuum forming after circuit attachment [43] is an alternative technique to handle more curvilinear shapes than origami folding geometries, it can hardly handle undercuts (e.g., twists and coils).

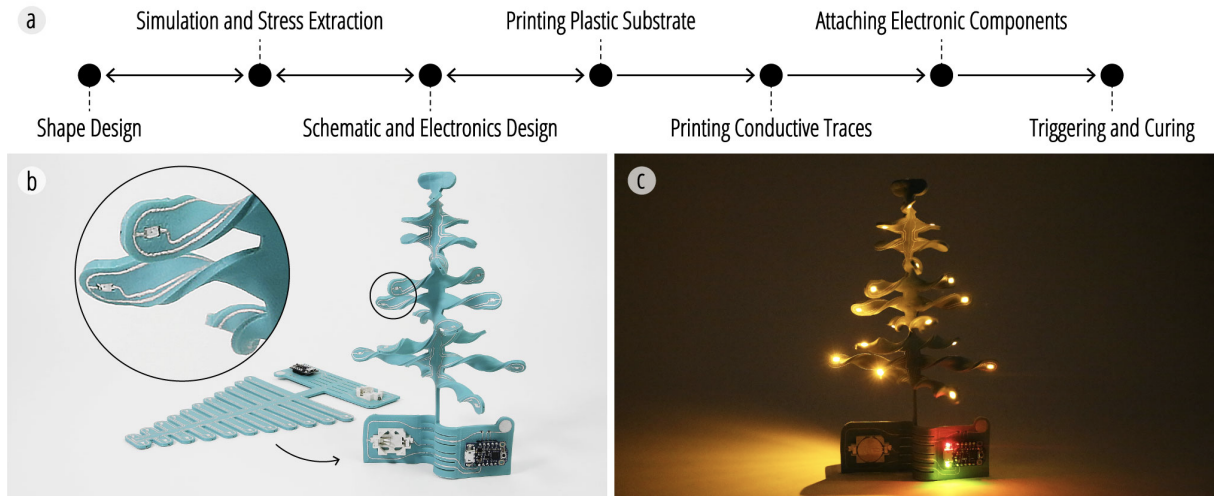


Fig. 1. (a) MorphingCircuit workflow; (b) a flat, as-fabricated artifact morphs into the interactive Christmas Tree; (b) demonstration of the interactive Christmas Tree in use.

To address the above mentioned challenges in manufacturing 3D conformal electronics, we propose MorphingCircuit (Fig. 1) which offers the HCI community a comprehensive approach including computational design, simulation, and fabrication to robustly and easily make self-morphing 3D circuits. Here the morphing occurs during the manufacturing process—a flat sheet can self-morph into 3D. The morphed part will then remain fixed in shape without further transformation when used.

We inquired about popular online PCB manufacturers such as OSH Park¹ and Sunstone Circuits² for the cost of rigid and flexible PCB printing, as well as resources needed to perform vacuum forming and 3D printing of functional electronics. The approach presented in this work has its unique advantages over existing circuit fabrication techniques. Particularly, it is an inexpensive and promising technique for attaching circuits to complex curvilinear surfaces. A detailed comparison is provided in Table 1.

Table 1. Comparison between MorphingCircuit and other circuits fabrication techniques.
(SMT: surface-mount technology)

Technique	Geometry	Cost (\$/cm ²)	E-Waste	SMT-Compatible
Rigid PCB ^{1,2}	2D	~\$5	Yes	Yes
Flexible PCB ^{1,2}	2.5D	~\$20	Yes	Yes
Vacuum forming PCB [45]	2.5D	~\$100	Yes	Yes
3D printing electronics [10]	3D	~\$100	No	No
MorphingCircuit	3D	~\$0.5	No	Yes

In this paper, we will go through the major design, simulation, and fabrication processes. Through a few applications, we show the breadth of functionalities and the complexities of shapes that can be achieved by this approach. The major contributions of the paper include:

- An accessible and inexpensive fabrication pipeline leveraging 4D printing to enable the embedding of electronics on complex 3D geometries such as loops, twists, coils, and metamaterial structure.
- A computational design tool that includes a tailored and precise morphing simulator complemented by a finite element analysis (FEA) model for predicting and optimizing silver trace placement.
- A set of interactive artifacts to highlight the capability of the MorphingCircuit for creating accessible, functional, and aesthetically pleasing electronics, with which we hope to inspire researchers, makers, and designers to use our approach for a wider range of applications.

2 RELATED WORK

Our work intersects with several areas in HCI, including fabrication, tools for fast prototyping, and shape-changing materials, which we discuss below.

2.1 Enhance Electronics with Fabrication

Researchers have leveraged novel fabrication techniques to create a wide range of passive tokens with integrated electronics to enhance their functionalities. These techniques create tokens as accessories with shapes that retrofit to existing electronics. Such tokens are often made from materials with special properties (e.g., conductive, magnetic, etc.), offloading sensing and computation to their host devices. For example, Acoustumment [27] designed a set of acoustic waveguides on smartphones to create an array of interactors. GaussStone [29] leveraged magnets to enable on-screen tangible interactions. Similarly, Flexibles [50] extended the sensing capability of a touchscreen to 3D space with conductive 3D prints. Fabrication has also been used to extend the sensing efficiency of electronics. For example, people have equipped capacitive sensing circuits with fabricated electrodes to fit complex everyday surfaces [14, 24].

¹ <https://oshpark.com/>

² <https://www.sunstone.com/>

2.2 Fabricate Interactive 3D Objects

Another common approach is to integrate electronics into 3D structures during or after the shape construction. One of the common approaches is to manually embed wiring and electronics into fabricated objects [20, 41, 60]. However, such manual processes could be laborious and inaccurate. In response, prior research has proposed a wide range of tools to facilitate the electronic embedding process after 3D shape construction for fast prototyping [47, 48, 74]. Researchers have also looked into printing traces or sensing primitives directly onto 3D printed objects. Capricate [49] proposed a design pipeline that allows users to easily integrate conductive materials in 3D objects for capacitive touch sensing. Printed Optics [67] prints optical paths inside 3D structures for sensing. FiberWire [55] uses carbon fibers together with plastics to fabricate 3D objects with embedded electrical routes. Although these systems aimed for a vision of fully automatic process of assembling 3D electronics, users still have to manually align electronics with the 3D shapes to some degree, which is challenging to be consistent and is incompatible with existing PCB manufacturing processes (e.g., pick-and-place). As a result, people have also looked for opportunities to assemble electronics onto 2D substrates, which can be subsequently conformed to 3D shapes.

2.3 Conforming Electronics to 3D Shapes

Electronics and 3D shapes can also be combined by conforming fully assembled, flexible circuits onto 3D shapes. One common approach is to print conductive traces as well as electronics onto paper that can be folded into complex shapes [25, 26, 38, 39]. Subtraction methods such as laser cutting [13, 73] and plotter cutting [69] have also been explored. Other researchers created circuits with conductive tapes and routes which can be easily attached to a wide variety of complex shapes for fast prototyping [17, 31, 44, 66]. It is also possible to create circuits on thermally deformable substrates, which can be molded into complex shapes with vacuum forming [42, 70]. However, this method does not support complex shapes since vacuum forming cannot easily handle geometries that have undercuts (e.g., twists, coil, and surfaces that have local minima). Finally, ShrinkyCircuits [30] uses prestressed polymer films that shrink when heated to improve the conductance of drawn traces and form into 3D shapes. However, its uniform shrinking method limits the controllability of local morphing parameters (e.g., shrinking rate and orientation) for complex 3D shapes.

2.4 4D Printed Shape-Changing Interfaces

Another body of research that is closely related to our work is 4D printing, which is a method to fabricate target 3D shapes via self-folding and self-morphing processes [4, 15, 35, 52, 53, 56, 58, 62-64], and it has drawn increasing attention in computational design and fabrication communities in HCI. For instance, Printed Paper Actuator [61] achieved reversible actuators and sensors with conductive thermoplastic materials. Transformative Appetite [64] pushed 4D printing technology to manufacture shape-changing food. Beyond HCI, biomimetic 4D printing [12, 18, 36], 4D printed robots [54], and reversible shape memory components [32, 68] have gained considerable interests recently. Among many existing works, the approach leveraging thermoplastic and desktop Fused Deposition Modeling (FDM) printers has gained popularity due to its accessibility. To summarize these FDM-based 4D printing work, we can divide the achievable shapes into two categories: developable shapes (i.e., shapes that can be flattened onto a plane without inherent distortion) such as A-line [63] and Thermorph [4], and non-developable shapes such as 4DMesh [62] and Geodesy [15]. To minimize the inherent material distortion and accommodate the silver ink traces (detailed in Section 4), MorphingCircuit can only achieve developable shapes. However, unlike A-line [63] that could only deal with 1D linear structures and Thermorph [4] that only integrates bending primitives to achieve origami-based geometries, MorphingCircuit extends the primitives into three types (bending, twisting, and coiling) and integrates both 1D lines and 2D sheets in its shape space. Additionally, none of the existing FDM-based 4D printing work has explored conformable electronics as an application context systematically.

2.5 Simulation in 4D Printing

To analyze the shape-changing process of a 4D printed structure, simulation is often used to predict the transformation and visualize the deformed structure. MorphingCircuit also features simulation to facilitate its use and therefore is related to prior work in this domain. There have been different types of simulation methods utilized in 4D printing. Thermorph [4], Printed Paper Actuator [61], 4DMesh [62], and A-line [63] adopt geometric simulation to predict the transformation, without considering the interactions between different parts of the structure. Geodesy [15] implemented the mass-spring model to simulate the structure's deformation, but the material's non-linear elastic behaviors, hyperelasticity, and viscoelasticity were not taken into account. In this paper, we implement a Finite Element Analysis (FEA) method to achieve an accurate simulation result. Similar to [72], we use FEA to predict the structure's deformation with predefined material definition, initial and boundary condition (i.e., residual stress), and tetrahedral mesh topology. Compared with the simulation tool developed in [72], we further extract the stress distribution map in order to visualize the recommended area for the silver trace location and to inform the electronic system design in the next step. Additionally, we wrap up the simulation pipeline with Python so that the tool is easily accessible to novice users with little FEA experience.

3 MORPHINGCIRCUIT DESIGN AND SHAPE SPACE

3.1 Design Space

MorphingCircuit takes inspiration from existing thermoplastic-based 4D printing technologies that adopt desktop FDM printers [4, 22, 59, 62, 63]. It was previously reported that printed plastic sheets shrink along the printing direction once triggered by heat. This phenomenon is driven by releasing the residual stress induced during the extrusion process and has been leveraged to program self-folding or morphing behaviors into printed sheets. Later in the simulation section, we will introduce our physical model that captures this stress-release and self-morphing process.

Compared to existing electronic products that require the PCBs to be embedded into 3D forms, our approach maximizes the integration of form and function within one manufacturing pipeline. Users can optimize form factors (e.g., aesthetic standards and space utilization of circuits on 3D objects) while building functional objects. Specifically, MorphingCircuit can be used in three application contexts:

- Conformal electronics on complex geometries: we demonstrate the achievable complexity of 3D shapes through an interactive Christmas tree with twisted branches ([Fig. 14](#)) and a meta-structural sensor design ([Fig. 16](#)).
- 4D printed robots: self-assembly robots have received increasing attention in both the academia and the industry. MorphingCircuit expands the fabrication boundaries of self-assembly robots by proposing a method that seamlessly combines shape design with functionality ([Fig. 15](#)).
- Customized electronic components: leveraging the inherent elastic properties of printed thermoplastic substrate, users can create reconfigurable or tunable electronic components, such as tunable capacitors, resistors, switches, inductors, etc. ([Fig. 13](#))

3.2 Shape Space

With the different combinations of the three actuator primitives ([Fig. 2](#)), we achieve a diverse body of shapes. For instance, the coils (e.g., inductors in [Fig. 13d](#)), branch twists ([Fig. 14](#)), and periodical twists ([Fig. 16](#)) exemplified in this paper are hard to achieve with other 3D electronic manufacturing methods that rely on vacuum forming [70], surface lamination [33], direct ink writing [30], or multi-material 3D printing [2].

The specific printing tool path directions and resulting bending angles of each actuator primitive are illustrated in [Fig. 2](#). For all three actuator types, they are constructed of two layers of the same thickness (0.6 mm) and each layer has a unique printing direction. In detail:

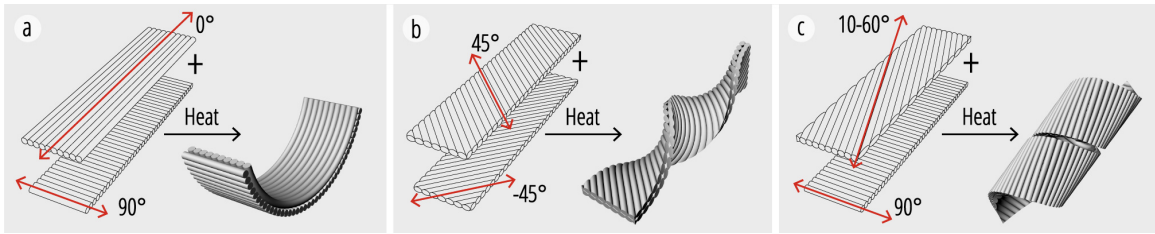


Fig. 2. Three types of actuators supported by MorphingCircuit: (a) bending; (b) twisting; (c) coiling. The red lines indicate the material shrinkage direction (i.e., printing path directions) upon triggering.

- The bending actuator (Fig. 2a) has one layer with a 0° print path relative to its longitudinal axis and the other with a 90° print path. Users cannot change the print path orientations for the bending actuator, but they can adjust the bending angle by adjusting the total length of the actuator with a set bending angle per unit length (i.e., 3.5 °/mm). Users can also choose either an upward or downward bending by alternating the order of the two layers.
- The second actuator type is the twisting actuator (Fig. 2b), which has a 45° and -45° print path relative to its longitudinal axis for each layer respectively. Users can alternate the two print path orientations to achieve either a clockwise or counterclockwise twist. The twisting angle can be adjusted through the width of the actuator through an iterative design process. As a reference, a twisting actuator with a width of 10 mm can achieve a 4.2 °/mm twisting angle. By increasing the width, we can decrease the twisting angle. The accurate twisting result will be presented to the user via our simulation platform detailed in the next section.
- The coiling actuator (Fig. 2c) has one layer with a 90° print path relative to its longitudinal axis, and the other with an optional degree ranging between 10° to 60°, with 60° having the largest coiling angle of 6.6 °/mm. We chose this particular range as it provided effective coiling based on our experiments. Additionally, by alternating the two layers, either a clockwise or counterclockwise coiling can be achieved.

4 DESIGN, SIMULATION, AND FABRICATION PROCESS

MorphingCircuit is enabled by a multi-step manufacturing process (Fig. 3), including pattern generation, simulation, schematic design, fabrication, electronic assembly, and a self-morphing process. We now describe the design and fabrication steps in detail.

4.1 Design and Simulation

Step 1: Shape and Printing Path Design (Fig. 3a)

The design of MorphingCircuit is a forward design process conducted in Rhinoceros, a 3D modeling software. Users start by creating a profile of a 2D substrate with a certain thickness. Although all our experiments are based on the substrate thickness of 1.6mm, our pipeline supports other thickness variations (i.e., 1.4 mm - 2 mm) as well. As the next step, users can divide the substrate into multiple sections and assign an actuator type for each chosen block. The non-assigned blocks will be considered as passive blocks and will be printed with a grid-based tool path that has no morphing potential [62]. There are three types of actuators users can choose from, including bending, twisting, and coiling actuators (Fig. 2). Since novice users may not have the prior knowledge to design shapes with the desired morphing behavior, the aforementioned details in the subsection 3.2 of shape space (Fig. 2) may serve as a guideline and help users to go through a more efficient iterative design process. For example, knowing the increase in actuator length will result in an increased bending angle; users can then shorten the actuator accordingly if they found that their simulation resulted in a bending angle that was too large. In this case, a trial-and-error through iterative designs between Step 1 and 2 will become a learning process for the user. We will explain the simulation tool next.

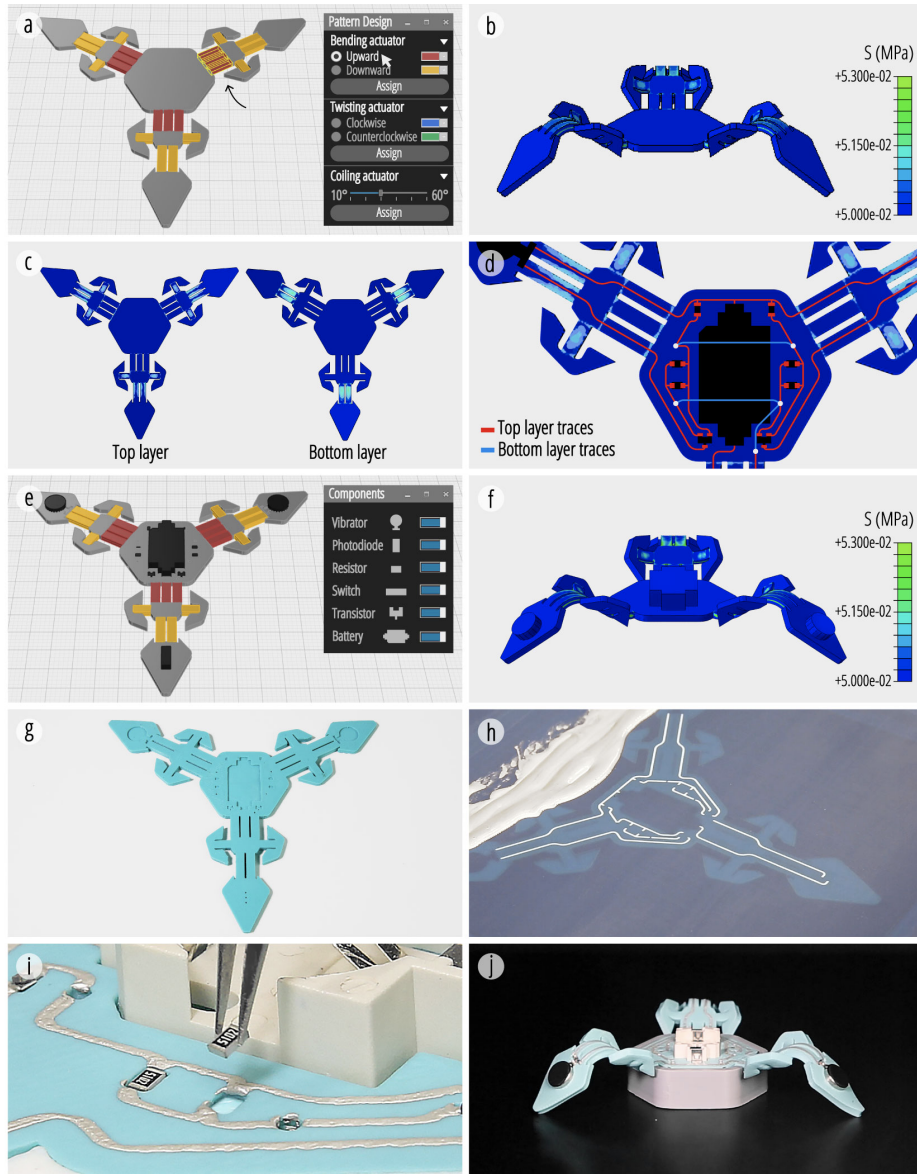


Fig. 3. Design, simulation, and fabrication overview. Users can (a) design the pattern and path in a 3D modeling software; the finite element based simulation of the design can predict (b) the structure's transformation and (c) stress distribution for (d) the traces and electronics design; users can (e) revise the 3D models with electronics integrated and (f) simulate the transformation of the revised model considering the influence of the electronics' gravity; (g) the 3D printed flat substrate can be easily (h) screen-printed onto with conductive trace and (i) attached with electronic components; (j) the flat electronic substrate self-morphs into a robot.

Step 2: Morphing Simulation (Fig. 3b)

To help users to simulate the morphing behavior and facilitate their iterative design process, we developed a precise simulation tool based on a finite element simulation strategy [72] to obtain the transformation result of the designed structure in Step 1. Users can import the 3D model from Step 1 into our simulation platform with

a .sat format. Fig. 3b shows the simulation result of a light-tracing robot. In practice, users can iterate between their 3D model design (Step 1) and simulation (Step 2) to achieve their desired final shape before printing. We will further explain how the simulation tool works in Section 5.

Step 3: Stress Extraction for Silver Printing (Fig. 3c)

Since the silver trace added on top of the 3D printed plastic piece may induce mechanical anisotropy [57] and affect the 4D transformation, our simulation tool also suggests preferable areas where silver can be applied. Specifically, we extract the stress distribution results from the FEA model of a designed sample and match different stress amplitudes with different colors. A stress distribution map is overlaid on top of the geometry, and the minimum-stress area is depicted by darker blue (Fig. 3c), which is the preferred area - also called the golden area - to align and print the conductive traces.

Step 4: Design Schematic (Fig. 3d)

Once the design of the plastic substrate is finalized, the next step is to design PCB schematics. Utilizing the simulation result, we route the traces accordingly in the EAGLE software to implement the electronics while maintaining the transformation quality. As shown in Fig. 3d, the circuit is drawn in Adobe Illustrator after exporting the .dxf file of the circuit traces from EAGLE. The optimized trace distribution consists of traces on both top and bottom sides and can be used for double-sided circuitry design.

Step 5 and 6: Revised 3D Models and Simulation with Electronics Integrated (Fig. 3e-f)

After the electronics are attached to the model, users can run the FEA simulation again to validate the morphing behavior and iterate through the geometry and circuit design if necessary. This revision step is to compensate for the potential influence of the weight of heavy electronic components to the original morphing effect simulated in Step 2. The weight of most electronic components are light-weight and have negligible effect on the sample's deformation (Fig. 3f), and even the heaviest one (i.e., the vibration motor) we used is less than 1.2g. Besides, we recommend placing the components at deformation-free regions based on the stress map in Step 3, since it further mitigates the weight's impact on transformation. However, we assume there will be a more significant influence if the components are much heavier. In this case, additional weight will be attached at the corresponding location of the substrate, and the simulation will be re-conducted in order to account for the gravitational effect.

4.2 Fabrication

Step 1: Printing Plastic Substrate (Fig. 3g)

We employ a standard 3D printing machine (MakerBot Replicator 2X) and common thermoplastic material (Polymaker PloyMax PLA) for the substrate fabrication. All the samples are printed at speed 4000 mm/min, printing temperature 200°C, with 60°C printing bed heating, 0.1 mm layer thickness, and a 0.4 mm nozzle. We design features such as sinks (Fig. 8a) and holes (Fig. 8b) on Polylactic Acid (PLA) substrates to hold surface mount devices (SMDs) and through-hole components and print them as part of the substrate.

Step 2: Screen Printing Conductive Traces (Fig. 3h)

Since the printed plastic substrates are smooth and flat, users can easily apply conductive traces with the standard screen printing process. In our case, we use pre-coated screen stencils (EZScreen HiDef Stencils) to customize the circuit pattern and commercial silver ink (CI-1001 from Engineered Materials Systems, Inc) to produce the traces. CI-1001 was chosen for its accessibility (off-the-shelf), flexibility and water resistance after curing; it was formulated specifically for screen printing and has a low resistance (<0.015 Ohms/Sq/Mil) suitable for functional circuits. In the future, to further increase the flexibility of the conductive ink and lower its influence during the morphing process, we may explore other customized inks including elastomer-silver composites [51] and elastomer-liquid metal composites [5]. For printing double-sided circuits, we design a holder and a spacer to hold the PLA substrate so that the bottom-side circuits will be printed first to preserve the printed silver traces.

Step 3: Attaching Electronic Component (Fig. 3i)

After printing the conductive traces, users then attach the electronic components. We design sinks on the plastic substrate to encase the electronic components, which are printed together with the substrate. Users can apply extra silver ink to the connection points between components and traces to make robust electrical connections. Due to the limitation on screen printing resolution, the minimum size of the SMD component we used is 1.6 mm x 0.8 mm and the minimum distance between two components should be larger than 1.2 mm. Since the plastic substrates are flat, we envision our assembling step to be fully automatic in the future with pick-and-drop PCB assembling machines.

Step 4: Triggering and Curing (Fig. 3j)

For our experiments and applications, we use two triggering methods, hot water and oven, to tailor to different shapes and conditions. We use 90 °C for both conditions. The 3D deformation and silver ink curing took roughly 3 minutes in hot water or 8 minutes in an oven to complete. Specifically, the hot water triggering method described in literature [62, 63] can be applied to waterproof components or for the case that allows post electronic assembly after triggering. Here we introduce the oven trigger method that can be more widely applied to the self-morphing process of electronics that are not waterproof. In the Performance section, we will compare the influence of silver trace conductivity by these two triggering methods.

5 SIMULATION TOOL

To assist the computational design and fabrication, we develop a simulation tool based on the FEA platform of Abaqus and the residual-stress releasing mechanism [62, 72]. Specifically, this mechanism achieves desired transformations by specifying the printing path direction of each layer, which determines the direction of the total shrinkage. While the underlying material model is based on [72], the simulation tool in this paper further extracts the stress distribution map from the simulation result and harnesses it to inform the electronic system design in the next step. To cater our simulation tool to different types of users, we customize a Python solver to bridge between a CAD design tool that is common among designers and Abaqus that is often used by expert users.

5.1 Functions

5.1.1 Transformation Simulation. The simulation tool can incrementally calculate the transformation of the structure, thus the final shape of the structure can be predicted and visualized by this tool.

5.1.2 Stress Extraction for Silver Printing. Our tool can suggest the areas where silver printing can be applied. Since our transformation prediction does not take the additional silver traces into account, we need to apply the silver ink to the areas that have minimum shrinkage, which corresponds to the areas that have minimum stresses and can be visualized through our tool.

Since the stress on each node of the FEA model is calculated, the simulation tool can extract the stress matrix from the simulation result and subsequently visualize the stress distribution map onto the geometry by following nodes' position. In this tool, a color code is used to represent different values of stresses and thus visualize the stress distribution map on the designed geometry.

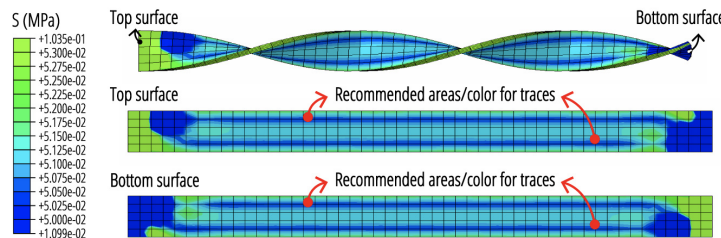


Fig. 4. The stress distribution map of a twist.

For example, Fig. 4 shows the transformation and the corresponding stress distribution map of a twisted sample. The dark blue color represents the minimum-stress area, which is also called the golden area. Silver traces should align and be printed on the golden areas since they experience the least amount of stress, and as a result the transformation of the sample will be least influenced.

5.2 Simulation Setting

Our simulation tool is built on a common simulation platform (i.e., Abaqus). To lower the barriers of technical simulation settings for general users, we customized a Python script to read in CAD models from Rhinoceros and automatically yield the simulation result by calling Abaqus to compute the simulation (Fig. 5a). The accessibility of our simulation tool to users who do not have FEA or Abaqus experiences is largely improved by this pipeline.

Since Abaqus needs many initial condition settings, to lower the barriers of technical simulation settings for general users, we convert the key settings required in Abaqus into the CAD settings in Rhino (Fig. 5b-d):

5.2.1 Setting of Geometry Orientation for Gravity (Fig. 5b). The orientation of the geometry determines the gravity's direction in the simulation model. Our simulation tool is based on the default global cartesian coordinate system in the CAD interface, thus users only need to set the orientation according to the sample's position in the experimental actuation process.

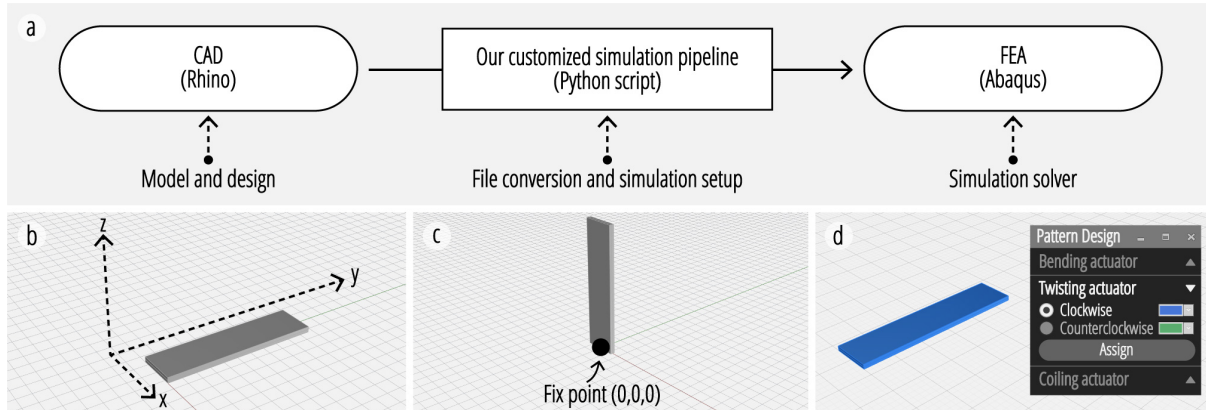


Fig. 5. (a) User workflow in the CAD interface, with (b) the geometry orientation setting, (c) the fixation setting, and (d) the different color settings to indicate different residual stress directions.

5.2.2 Setting of Fixation (Fig. 5c). To remove the sample's rigid body translation in simulation, we need to fix a point on the sample. The position of the sample's fixing point should follow the boundary conditions (i.e., the gravity) of the sample in the triggering experiment. When the position of the fixing point on the CAD geometry is identified, users should move this point onto the origin of the predefined global cartesian coordinate system. This fixing point is also the position of the fixation boundary condition in the simulation model.

5.2.3 Setting of Stress Alignment (Fig. 5d). In CAD interfaces, users should define the stress direction (i.e., the orientation of the printing toolpath) in the geometry. Since the two layers (i.e., the top and bottom layers) commonly have different residual stress directions, users need to specify an angle for the stress direction based on the predefined local cartesian coordinate system. Users can use different colors to represent different directions.

After users finish the above settings, they can then export the CAD design into a file with the .sat format that will be imported into our customized simulation platform implemented in Python. Our Python script connects CAD users with Abaqus as the simulation solver seamlessly. We will explain the simulation physical

setups in Section 5.3. We suggest the format of “Part#_angle.sat” for the naming to make it interpretable by our Python script. For example, for a bi-layer structure that consists of two parts, it will be exported into two separate files named with “Part1_45.sat” and “Part2_90.sat” respectively, where the part number indicates the order of layers from the top, and the digits indicate the printed angles.

5.3 Python Pipeline Implementation

The Python pipeline takes a .sat file as the input and handles the material definition, geometrical meshing, initial and boundary conditions setup, and sequential simulation. The code of this encoded Python pipeline is provided in the Supplementary Material. Fig. 6 depicts the sequential steps of the pipeline implementation. All steps are elaborated in a subsection as follows:

5.3.1 Geometry Establishment and Partitioning. The geometry of a designed structure and the layer partition information is extracted from the .sat file and processed through the Python script to be read by Abaqus. Based on the original geometry (Fig. 6-step 1), the pipeline can automatically generate partitions to create a bilayer structure (Fig. 6-step 2) with respect to the thickness direction.

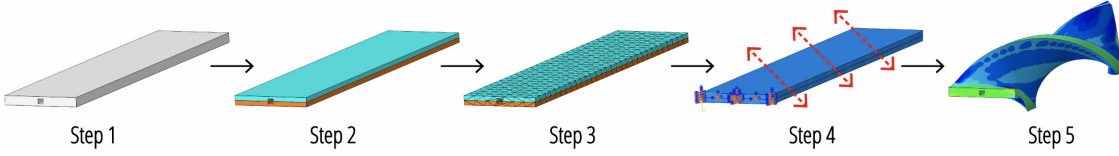


Fig. 6. The process of pipeline implementation. Step 1: Import the geometry; Step 2: Partition the geometry and define material properties; Step 3: Discretize the geometry with tetrahedral mesh; Step 4: Initialize the shrinkage direction and the fixation point; Step 6: Simulate the transformation and visualize the result.

5.3.2 Material Definition. To accurately simulate the structure’s deformation, we leverage the dynamic mechanical analysis of PLA conducted in [72] to complete our material definition. The pipeline considers both the hyperelastic and viscoelastic behaviors of the PLA since the triggering temperature is higher than its glass transition temperature (T_g) [8]. With the built-in feature of Abaqus, we then integrate the experimental data from [72] into the FEA model right after the geometry partitioning to define the material’s hyperelasticity and viscoelasticity.

5.3.3 Meshing. We choose the tetrahedral element as the mesh type to build the discretized simulation model (Fig. 6-step 3). This type of mesh can handle multiple complicated topologies, and it can generally maintain the simulation accuracy.

5.3.4 Initial Condition and Boundary Condition. In order to capture the physical material structure and triggering condition, we need to set up the initial and boundary conditions in the simulation (Fig. 6-step 4). First, we need to rotate the residual stress based on the local direction of the printing path (denoted as σ_{rot}). The residual stress of different parts can be decomposed into several stress vectors due to their different relative coordinates within the structure, and can be described by following the equation of Cauchy stress tensor [45]:

$$\sigma_{rot} = R \cdot \sigma_x \cdot R^T$$

$$R = \begin{bmatrix} \cos\theta & -\sin\theta & 0 \\ \sin\theta & \cos\theta & 0 \\ 0 & 0 & 1 \end{bmatrix}, \sigma_x = \begin{bmatrix} \|\sigma\| & 0 & 0 \\ 0 & 0 & 0 \\ 0 & 0 & 0 \end{bmatrix}$$

where σ_x denotes the matrix of the stress field along with the printing path direction ($\sigma = 0.178$ MPa), θ denotes the angle between the printing path direction and the x-axis of the global coordinate system, and R is the rotation matrix.

We also have to set the fixation point - which may have different positions for different structures - in the FEA model as boundary conditions (the closest end of the beam shown in Fig. 6-step 4). This fixation point should correspond to the actual fixed point when we trigger the physical structure.

In an actual user workflow, both initial and boundary conditions are set inside CAD and passed down to Abaqus through our Python solver as previously explained in Fig. 5.

5.3.5 Simulation Sequence. In the 90 °C triggering environment, the PLA structure may get softened in the first place, and then release its embedded residual stress. Thus, the actual transforming process can be divided into 1) the body force creeping, and 2) the residual stress releasing. In the simulation, we create two separate FEA models corresponding to the two separate experimental processes. We simulate these two models in a sequence: first simulating the intermediate transformation with the body force (Fig. 7b) and second simulating the final transformation after the residual stress has released (Fig. 7c). The simulation sequence is conducted in the pipeline by calling the FEA solver (Fig. 6-step 5).

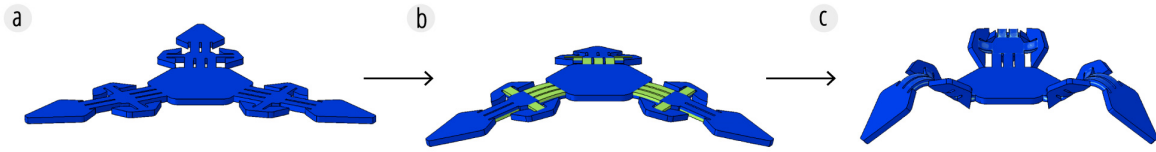


Fig. 7. The simulation result of the sequential transformation: (a) the initial geometry; (b) the intermediate transformation under the influence of body force creeping; (c) the final transformation after residual stress releasing.

With the above steps, the pipeline can be characterized by the following pseudo-code:

ALGORITHM: Pipeline for Automatic FEA Execution

```

Input: Geometry,  $G$ 
Partition the geometry  $G$  into  $G_1$  and  $G_2$  // define the bi-layer structure
if electronic component design location is specified then
    Add a block at the component's position // block should have the same weight as the component
    Integrate additional blocks into  $G$ 
end
Generate node set  $N$  with label based on the geometric boundary of  $G_1$  and  $G_2$ 
for each  $N_i \in N$  do // node set definition
    Gather coordinate tuple  $p_i = (N_{ix}, N_{iy}, N_{iz})$ 
    Gather adjacency information with nearby nodes  $A_i$ 
    Assign  $(p_i, A_i)$  to  $N_i$ 
end
for each  $(p_i, A_i, N_i) \in N$  do // element set definition
    Connect  $N_i$  with other nodes based on  $A_i$ 
    Compute Gaussian integration point coordinates  $g_i$  based on  $p_i$  // used for stress calculation
    Generate element  $E_i$  to form element set  $E$ ,  $E_i = (p_i, g_i, A_i, N_i)$ 
end
for each  $(N_i, E_i) \in (N, E)$  do // mesh generation
    Generate mesh structure  $M$ 
end
Define material property  $H$  on mesh  $M$  //  $H$ : density, hyperelasticity, viscoelasticity, ...
Establish FEA solver setting  $S$  // define simulation step size, increment number, converging threshold, ...
Define boundary condition  $BC$  on node set  $N$  //  $BC$ : gravity, end fixation, ...
Define initial condition  $IC$  on node set  $N$  //  $IC$ : residual stress for each layer
Generate mesh modeling file,  $F = (N, E, M, H, S, BC, IC)$  //  $F$ : integrate FEA model definition

```

Submit \mathbf{F} to the Abaqus FEA solver // Execute the simulation on Abaqus

Save deformation and stress results, \mathbf{D}, \mathbf{T} .

Update node set, element set and mesh structure with new position, $\mathbf{N}^*, \mathbf{E}^*, \mathbf{M}^*$.

Output: Simulation result file, $R = (\mathbf{N}^*, \mathbf{E}^*, \mathbf{M}^*, \mathbf{D}, \mathbf{T})$

To facilitate others' easy access to our system, we have open-sourced this project in Github³.

6 DETAILED FABRICATION TECHNIQUES

We describe the fabrication details to help users simplify the assembly process and improve the fabrication quality (Fig. 8). Most of these structural features are easy to achieve and do not need additional manufacturing time due to the chosen 3D printing process.

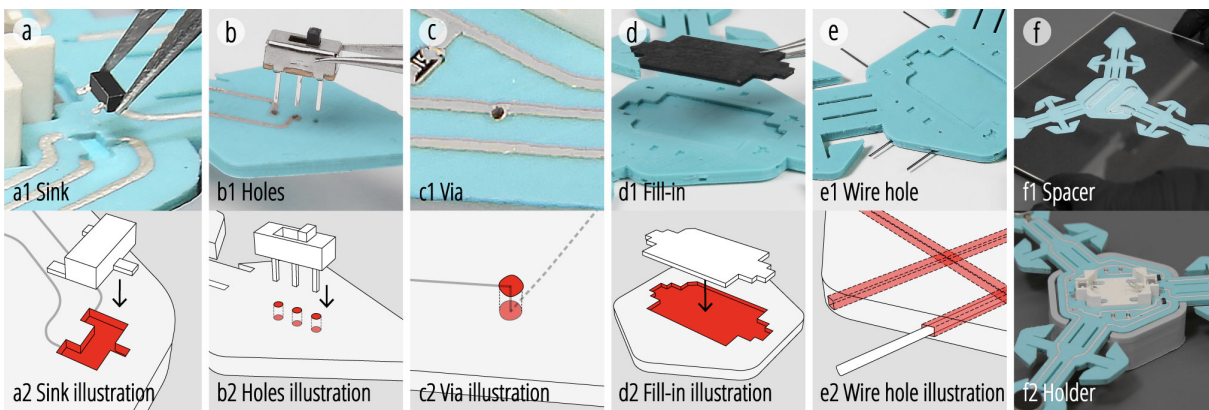


Fig. 8. Fabrication details: (a) sink; (b) holes; (c) through-hole vias; (d) filling-in components to ensure the flatness of the substrate; (e) hollow support channel; (f) spacer and holder for double-sided printing.

6.1 Sinks for Electronic Components Allocation (Fig. 8a)

We design sinks to host the electronic components. The sinks make the electronic placement easy and precise. Additionally, the mechanical boundaries of the sinks make the components attached more securely, and they can prevent the components from falling off during the transportation or triggering process.

6.2 Holes for Electronic Components Assembly (Fig. 8b)

We print holes for through-hole components such as the switch to allow secure attachment. The size of holes are designed to match the pin size of through-hole components. After triggering, holes will further shrink to ensure secure connection. The effectiveness of connection can be tested by a multimeter.

6.3 Through-hole Vias for Double-sided Circuits (Fig. 8c)

In order to make better use of the space of the flat substrates and distribute traces to the golden areas based on the simulation suggestions, we set up the vias to achieve the double-sided circuits design. The vias can be generated using the auto-routing function in EAGLE, and users can modify the original models to adjust vias in the CAD software.

³ <https://github.com/Anonymo-lab/MorphingCircuit-simulation-pipeline>

6.4 Filling-in Components for Screen Printing (Fig. 8d)

Keeping the substrates flat during screen printing is critical for achieving high-quality traces. However, the sinks we designed to host the electronic components create unevenness on the substrate surface. We 3D print a flat sheet in the form and thickness of the sink to temporarily fill it, and make the substrate a uniformly flat surface before the ink is applied.

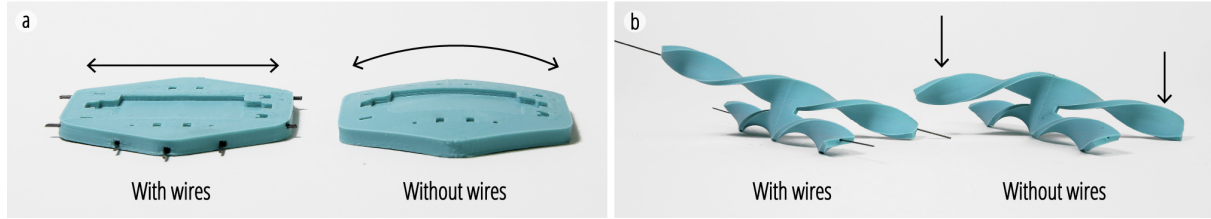


Fig. 9. The experimental verification of the benefit from the embedded wires. (a) The embedded wire prevents the sample from popping up. (b) The wire enhances the sample's bending stiffness against the body force, thus removing the sample's deflection in the radial direction.

6.5 Hollow Channels for Embedding Wires to Minimize Gravitational Effect (Fig. 8e & Fig. 9)

Gravity may induce undesired deformation and subsequently influence the final shape of the sample. Adding sugar into hot water can compensate for the gravitational effect to some extent [62, 63]. However, it was not as effective for large and heavy samples. In reference to the method described in [7], physical properties of 3D printed materials can be changed by embedding other materials. Therefore we recommend embedding multiple thin metal wires (0.5 mm in diameter) into flat and heavy structures (Fig. 8e) which deform the least (i.e., the passive area) as well as the twisting structures with a length longer than 80 mm to increase their stiffness during triggering, thereby reducing the effect of gravity and body force. Hollow channels (cross-sectional dimension: 1mm x 1mm) could be designed manually in the design process. As shown in Fig. 9a, the shape with wires embedded can maintain the flat state than the one without wires during the trigger process. For the twisting shape, the central axis of the twist can be strengthened by wire embedding. Fig. 9b shows that the wire can help reduce unwanted gravitational effect during the triggering process.

6.6 Spacer and Holder for Printing Double-side Traces (Fig. 8f)

Since silver ink is sticky before curing, it is necessary to make sure the silver traces are intact during the assembly and triggering process. Therefore, we suggest adding spacers (Fig. 8f top) to lift up the side that has already been applied with silver traces before the substrate is flipped to the other side to be printed onto. Alternatively, if we want to keep the silver traces intact during the triggering process, we can also customize a holder to lift up the sample from the ground. For example, we customized a holder to hold a self-morphing robot in the oven during the triggering process (Fig. 8f bottom).

7 EVALUATION

In this section, we evaluate both the accuracy of simulation and the performance of fabrication methods.

7.1 Simulation Accuracy Evaluation

To evaluate the accuracy of simulation, we pick three deformation primitives and the light-chasing robot as validation samples and follow the evaluating strategy of [72] to measure the distance or angle difference between several points or edge pairs. The points or edge pairs are depicted in Fig. 10a and Fig. 10b. The detailed measurements are included in Fig. 10c, where the experimental result of each validation sample is obtained by

taking an average of three different measurements. Since we apply the silver trace on the structures' golden areas, we believe that the weight and non-linear material properties of silver traces have minimal influence on structural deformation. This implies that the silver trace-free simulation should have a high accuracy for deformation prediction compared to the real deformed sample with silver traces applied.

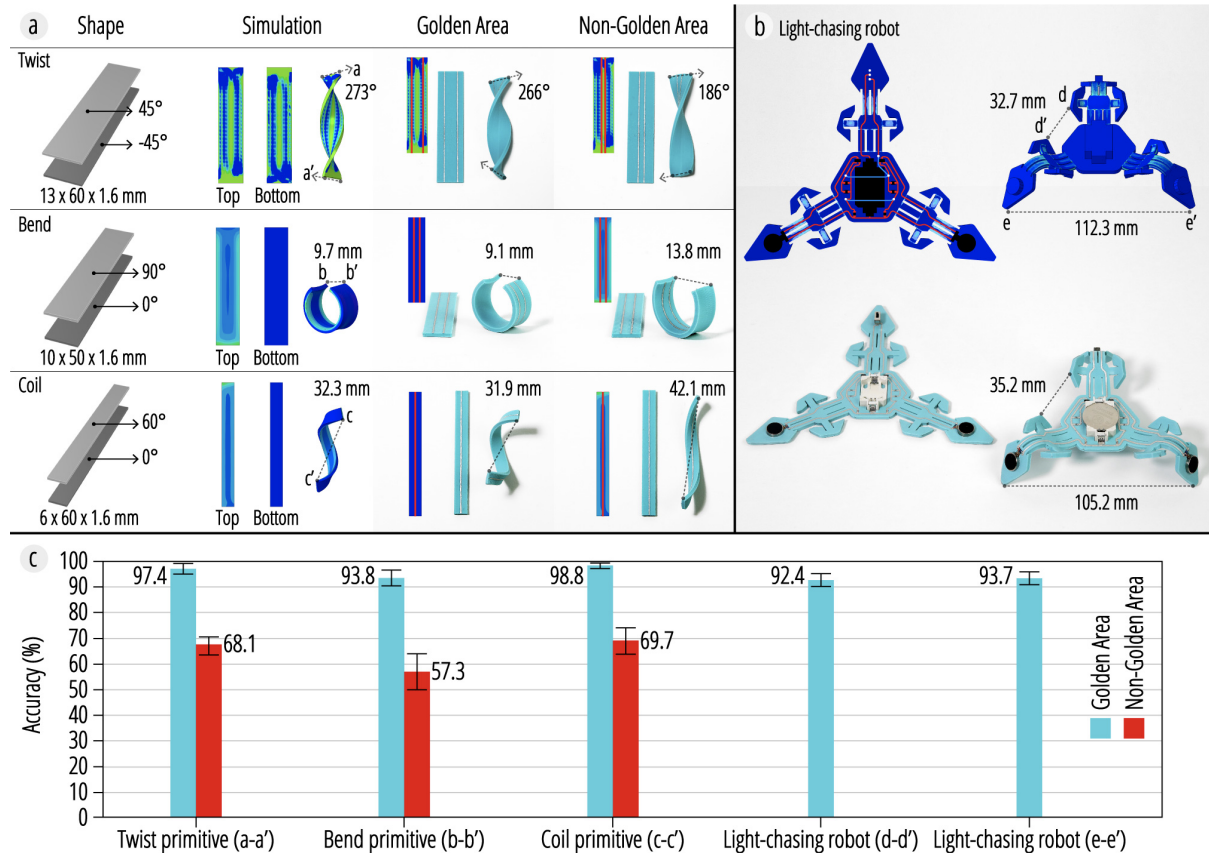


Fig. 10. Simulation evaluation of (a) three deformation primitives and (b) the light-chasing robot. Each sample is assigned with points or edge pairs (depicted by dots and lines) and evaluated by comparing the translational/rotational displacement in simulations and experiments. (c) shows the detailed accuracy results, which are obtained by dividing the difference of displacements between simulation and experiment by the corresponding displacement in simulation; blue bar: samples with silver traces applied on the golden area, red bar: samples with silver traces applied out of the residual stress areas.

The results in Fig. 10c show that, with silver traces applied on the golden area, the true deformation of validation samples comes close to the prediction of silver trace-free simulations. If the silver traces are misplaced out of the golden area, the deformation will be heavily influenced.

7.2 Silver Screen Printing Resolution

To evaluate the screen printing resolution, we print ten traces with a width ranging from 0.1 mm to 1mm on two pieces of PLA (Fig. 11) and repeat the printing three times. Overall, three samples show the same result that the highest resolution of traces is achieved with a width of 0.3 mm.

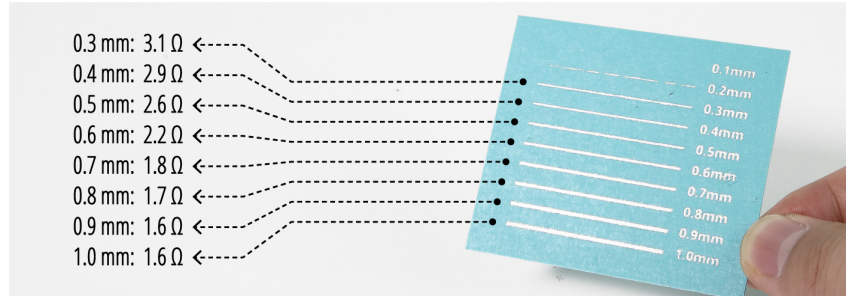


Fig. 11. Screen printing resolution. The resistance of the trace is negatively correlated with its width.

7.3 Silver Trace Conductivity

7.3.1 Triggering Method and Conductivity. We demonstrated two triggering-while-curing methods in previous sections - 3 minutes in a hot water bath or oven at 90 °C. To compare the conductivity of silver traces using our triggering methods with the curing method recommended by the silver ink supplier (i.e., curing for 10 minutes at 120 °C), we printed silver traces on a substrate that does not deform under our testing conditions and measured the resistance values for all three conditions. For each test, we have three samples. Fig. 12a shows comparisons between different conditions including oven triggering with the officially recommended temperature (120 °C for 10 mins) (S1), oven triggering under our experimental temperature (90 °C for 8 mins) (S2) and water triggering under our experimental temperature (3 mins in water) (S3). The resistance of the silver trace was almost identical for S2 and S3.

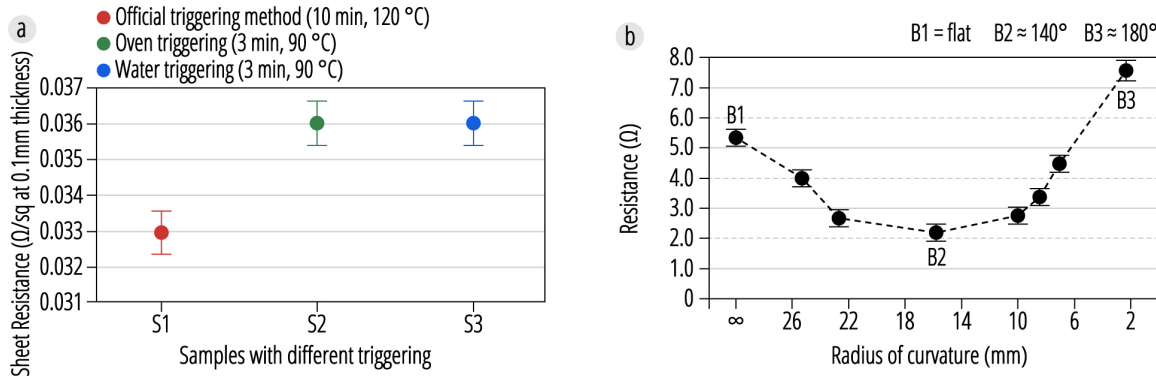


Fig. 12. (a) Comparison of silver trace performances under different triggering conditions. (b) Comparison of silver trace performances induced by the radius of curvature. All the testing traces in both (a) and (b) share the same dimensionality of 50 × 0.4 × 0.1 mm.

7.3.2 The Radius of Curvature and Conductivity. To evaluate how the morphing of our PLA substrate affects the conductivity of the silver trace (Fig. 12b), we analyze changes in the silver trace resistance induced by the different radius of curvature. We conduct experiments with the bending type strips (dimension: 45.89 x 9.49 x 5 mm). We printed silver traces on the inner side of the bending actuator and cure it with the officially recommended method. From Fig. 12b, we can obtain resistances at different radii: flat (5.3 Ω), 15.75 mm (2.23 Ω), and 2.35 mm (7.67 Ω). The results of the measurements are averaged values of three samples. The sample with 2.35 mm radius of curvature has a bending angle of 180°, in which case, the strip is folded in half. The

conductivity is lower yet the silver trace is not broken for this case. After a certain radius of bending curvature (140°), the resistance of silver increases at the bending point causing the overall resistance to increase.

7.4 Repeatability and Durability

To demonstrate good repeatability in the morphing performance, we printed all the demo pieces multiple times and compared the results (Fig. 13a). Additionally, to illustrate the repeatability in silver trace printing, we fabricate three identical tunable resistors. Fig. 13b shows that the differences in the measurement of resistance are less than 1%. For durability, all samples work well at room temperature (20°C - 30°C). We also tested the touch and hover sensing on the Christmas tree in one day, three months and eight months after the tree was fabricated. All the LEDs and the sensing function works well.

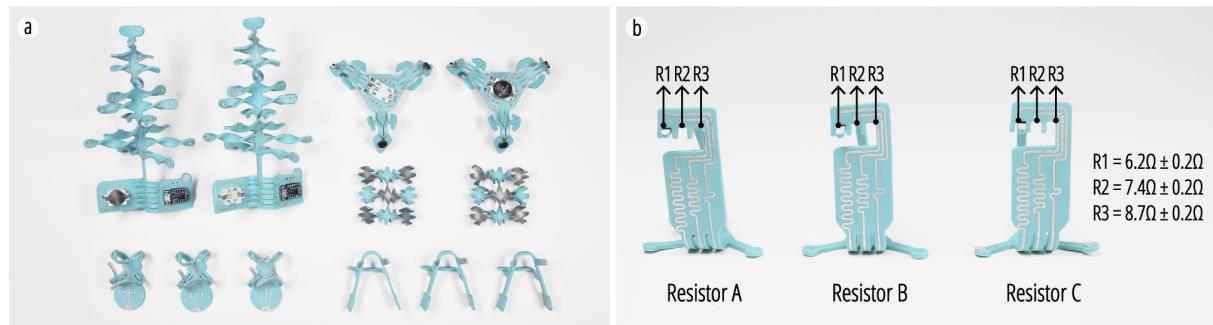


Fig. 13. (a) Result of the shape repeatability test. (b) Experiments show a high consistency of the trace quality and resistance value.

8 DESIGN CASES

MorphingCircuit is an integrated design, simulation, and fabrication approach for conformal electronics with complex substrate geometries through 4D printing. This method allows electronic structures to take on shapes that were previously difficult or impossible to design or manufacture. To demonstrate the versatility of this approach, we provide four different tunable electronics and three applications that are fully functional, with each demonstrating a different interactive function with varying geometric complexities (e.g., multiple twist surfaces, metamaterial structure, bending and coiling structure). Additionally, we try to stick to the design principle that form is the function. For example, a meta-structure is a soil scaffold as well as a moisture sensor (Fig. 17).

8.1 Morphing Components Design

To demonstrate the versatility of MorphingCircuit to implement electronic primitives that have tunable electronic properties and 3D shapes, we prototype four common electronic components: a capacitor, a resistor, an inductor, and a switch. Each component can be printed with a custom-shape and desired value range. Fig. 14 a-d illustrate the mechanisms of these components using MorphingCircuit approach and report measurements of each component. For example, a capacitor with three capacitance values of 0.86 pF , 1.13 pF , and 1.85 pF is fabricated as shown in Fig. 14b. It offers three choices of capacitance determined by the position of the inserted pin. Additionally, these primitives could be potentially modified with a wider range of electronic properties. Within the physical and materials limitation, users can iteratively explore designs beyond the demonstrated example and tune, for example, the capacitance to microfarad or millifarad range and boost the resistance to kilohms simply by changing the distribution of the silver traces.

In Fig. 14a, three of the four legs of the spider-like shape are corresponding to three negative terminals of an RGB LED, and the other leg is for the positive connection to the power source. By locking the legs in different positions, different colors will light up to demonstrate different on-positions of a switch. Similar mechanical switching mechanisms were used to design the tunable capacitor and resistor in Fig. 14b-c as well.

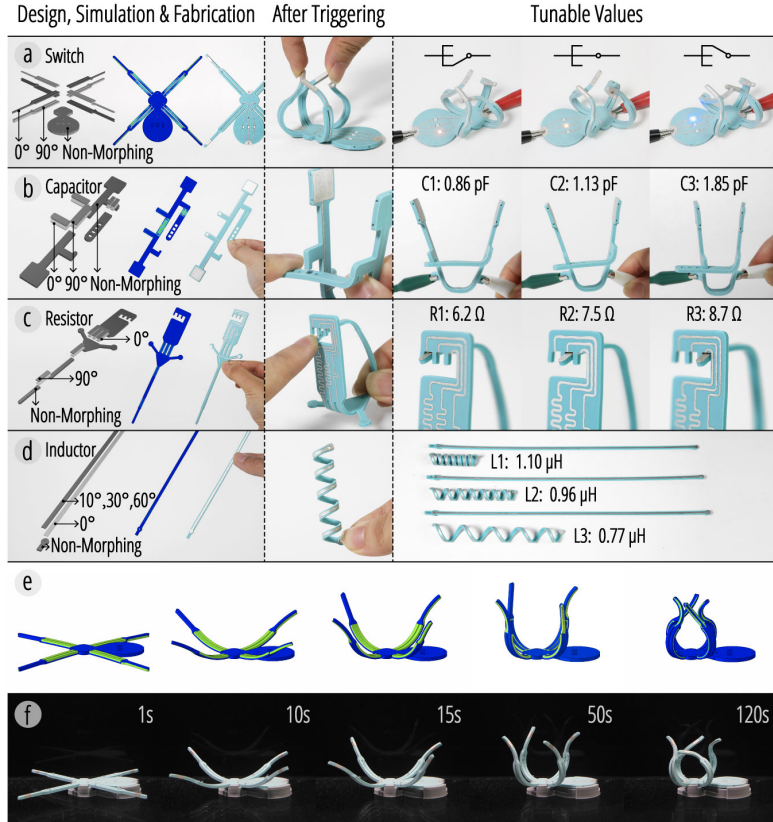


Fig. 14. Different electronic component designs: (a) a simple three-way switch (achieved by bending), (b) a tunable capacitor (achieved by bending), (c) a tunable resistor (achieved by bending), and (d) a tunable inductor (achieved by coiling). The result of the tunability test of each design is shown in the right column. (e) Simulation of the switch. (f) The printed switch self-morphing in hot water.

We use the parallel-plate capacitor structure to design the tunable capacitor (Fig. 14b). The capacitance decreases as the distance between two plates increases (Fig. 14b). For the design of the tunable resistor (Fig. 14c), we print different lengths of silver traces at three different locking positions. The resistance of the resistor increases as the length of the trace increases. The self-inductance of the solenoid is affected by the number of turns in the coil, the cross-sectional area of the coil, and the length of the coil. In Fig. 14d, we fabricated different shapes of coils as tunable inductors. Inductors 1 and 2 have the same number of turns and cross-sectional areas of the coil but inductor 2 is longer than 1, so inductor 2 has smaller inductance. The inductor 3 has the same cross-sectional area as inductor 2 but the longer length and less number of turns, so it has smaller inductance than inductor 2. All of our values of resistance, capacitance, and inductance were measured by LCR meter (LCR-600, 100 kHz LCR meter from Global Specialties).

Fig. 14e and f show that there is a subtle difference between the simulation and experimental results of the switch. We speculate that this difference is due to the application of silver ink, which is more significant than

the previous examples as compared to the switch's own legs. The extra weight possibly induces gravity creeping, leading to the discrepancy between FEA prediction and physical results.

8.2 Decoration Design: Interactive Christmas Tree

Following the design principle that “form follows function”, we design an interactive and portable Christmas tree with touch sensing and hover sensing as an integration of both design and function. The branches of the tree are achieved by twisting transformation; another function of the branches is to carry the connection traces for LEDs (Fig. 15). This branched twisting is hard to achieve with conventional 3D printing, injection molding, or vacuum forming technique.

This interactive tree has three modes. When the user first touches the silver panel, all LEDs turn on and after the second touch, the silver panel will sense the distance of the user's hand and the panel itself. The distance is visualized as the brightness of LEDs. After the third touch on the panel, all LEDs turn off.

The 3D-shaped Christmas tree is one flat piece when we assemble all the electronics components. It has the advantage of saving electronic assembly effort, space, and cost for fast packaging.

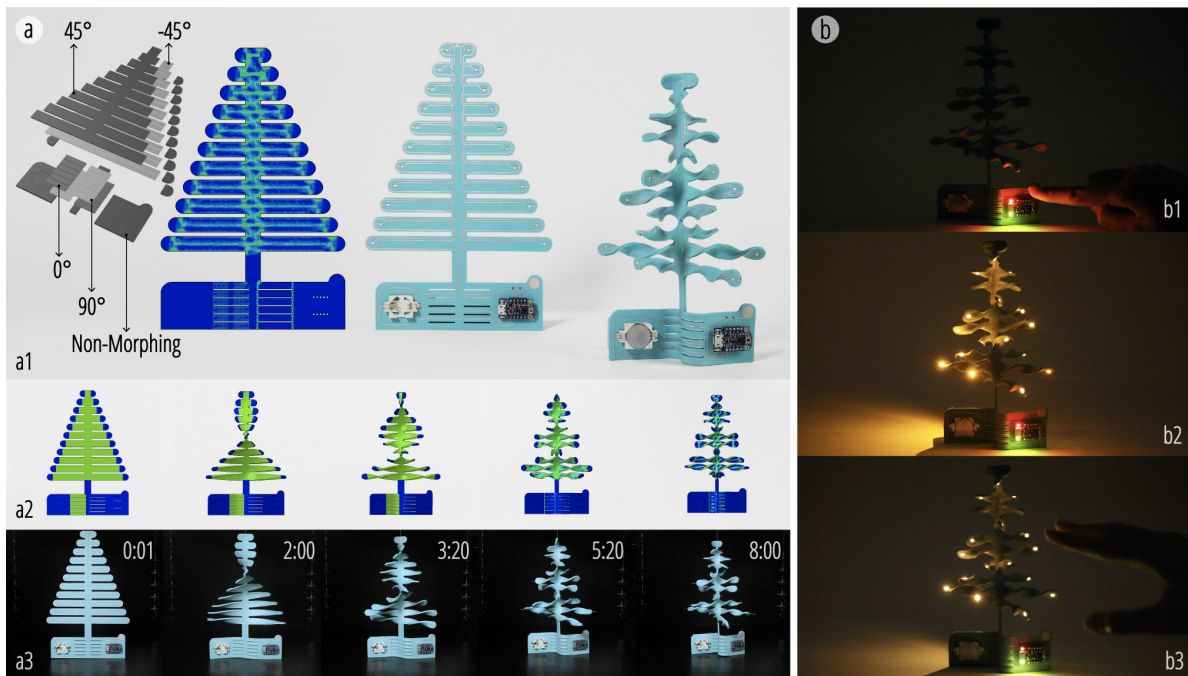


Fig. 15. Self-morphing Christmas tree. (a) a1: From left to right, it shows the layer construction of the substrate, the stress extraction for silver printing, the flat state after electronics assembly, and the final shape after morphing; a2: simulation of the transformation; a3: physical transformation triggered in an oven. (b) The interaction scenario.

8.3 Robot Design: Light-chasing Robot

We prototype a self-folding light-chasing robot with integrated surface mount photodiodes, transistors, vibration motors, and a battery (Fig. 16). The transistor operates as a “switch” for the motors. The robot is designed to follow the path of light. When light shines on a photodiode, the photodiode converts the light into current and provides voltage for the base terminal of the transistor, which then activates the corresponding motor.

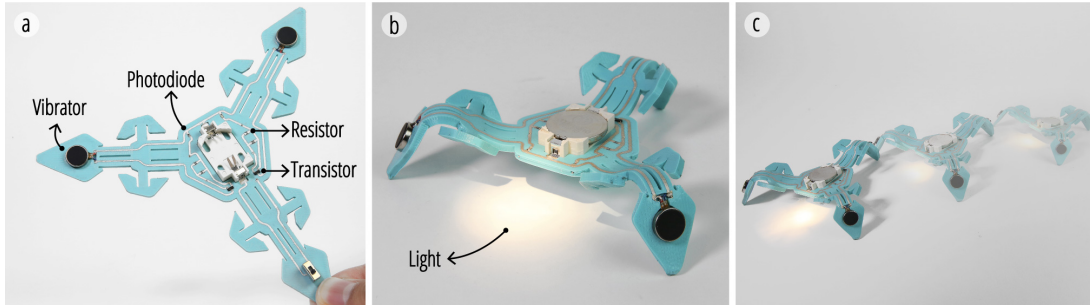


Fig. 16. Self-folding robot. (a) The electronic components used in (b, c) the light chasing interaction.

8.4 Sensing the Environment: Meta-Structural Moisture Sensor

Taking advantage of the large contact area and porosity of a periodical meta-structure shown in Fig. 17a, we develop a soil moisture sensor that also functions as a breathing scaffold for the soil. The biocompatibility of PLA substrate and platinum conductive coating makes the structure environmentally friendly.

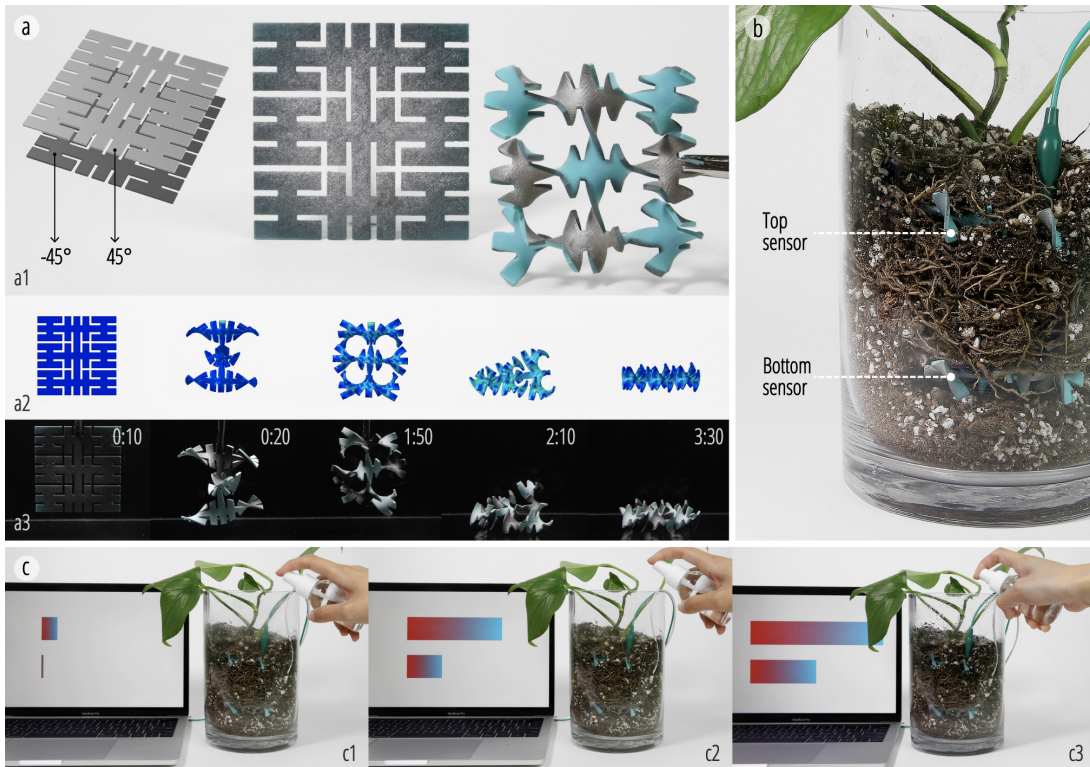


Fig. 17. Meta-structural moisture sensor. (a) a1: From left to right, it shows the layer construction of the substrate, the flat state with coating, and the morphed final shape; a2: simulation of the transformation; a3: physical transformation triggered by hot water. (b) Position of the sensors in the soil. (c) The interaction scenario.

In this application, instead of screen printing silver traces, we coat the meta-structure using a standard sputter coater (Quorum). The sputter coater forms a 5 nm thin platinum on the top surface. Compared with silver ink

printing, sputter coating has much fewer effects on the transformation and is environmentally harmless for biocompatible applications. However, it is less accessible and it will coat the entire surface rather than selected regions without additional masking procedures.

Using the meta-structure as a capacitive humidity sensor, we can detect the signal change in dielectrics, which is caused by measuring the concentration of ions dissolved in moist soil. Fig. 17c shows that when the user pours water to their plants, two bars for the upper and lower moisture levels are visualized. The top bar visualizes the moisture level of the upper layer of the soil. When the humidity level of the soil increases, the bar will also elongate horizontally. Because the water is spread from the top, the upper level of the soil is moister than the lower level of the soil as indicated by the difference in the bar length. The colors on the bars better visualize the moisture level change with the red color indicating lower moisture level and the blue color indicating higher moisture level.

9 DISCUSSION, LIMITATION, AND FUTURE WORK

Compared to existing fabrication methods, MorphingCircuit provides a low-cost and low-pollution alternative to fabricate PCBs for conformable electronics that have curvilinear substrates. Nonetheless, our technique is still at an early development stage and can benefit from addressing the following aspects:

9.1 Generalizability in Simulation

Our simulation tool is established based on the integrated FEA platform of Abaqus, which is not open or free. However, most of the research units may have an institutional subscription. Additionally, our algorithms and implementations can be adapted to other open-source FEA tools including LAMMPS, and other alternative tools that may be subscribed with a lower cost including COMSOL and ANSYS.

9.2 Simulation for Silver Traces

We currently omit the silver trace feature in our established simulation models for two reasons. Firstly, due to the non-constant material properties of the silver trace during the curing process, the material definition of the silver trace is difficult to characterize in our simulation tool. Secondly, since the weight of the silver trace is far lighter than the thermoplastics, we reasonably ignore the gravitational influence resulting from the silver trace. Future works may take the silver trace features into account to provide even more accurate simulations.

9.3 Design Iteration and Efficiency

All simulations demonstrated in this paper are completed using a consumer-grade CPU (8-core Intel I9-9900k @ 5GHz) within 15 minutes. Although this is not a real-time process, simulations still greatly minimize the time of a single optimization iteration compared to the physical prototyping without the assistance of a simulator, which may cost much more time to iterate through a trial-and-error process. Table 2 shows the comparison between simulation time and physical prototyping time.

Table 2 indicates that simulation can be much more time-efficient than physical prototyping methods, and the overall time accumulated from the initial design establishment to the final optimal design is minimized throughout the pipeline implementation. The high time efficiency of simulation can be leveraged to speed up the iterative design process; however, the time performance of the simulation process varies in different cases. For example, the simulation time of the Christmas Tree design is approximately 71.8 times shorter than its printing time plus triggering time, while the simulation speed of the inductor design is only around 1.5 times faster than its physical prototyping speed. Generally, the longer the printing time a design has, the more efficient the simulation is compared to physical prototyping in terms of time. When the printing time of one design is less than 10 mins, the physical prototyping may be as fast as the simulation.

Table 2. Time efficiency comparison within one iteration.

Application	Physical Prototyping Time			Simulation Time	Times Efficiency (Physical Prototyping/Simulation)
	Printing Time	Triggering Time	Total Time		
Switch	66min	3min	69min	2min 45s	~25.1x
Capacitor	45min	3min	48min	5min 24s	~8.9x
Resistor	28min	3min	31min	7min	~4.5x
Inductor	10min	3min	13min	8min 50s	~1.5x
Christmas Tree	456min	10min	466min	5min 42s	~71.8x
Light Chasing Robot	155min	10min	165min	18min 39s	~8.8x
Meta-Structural Sensor	58min	3min	61min	16min 40s	~3.7x

9.4 Integrated Design Pipeline

MorphingCircuit aims to offer a framework to support the forward design of transformative PCBs, but this process is not yet fully integrated and requires manual intervention. As a result, the current workflow requires the user to have a pre-installed FEA solver and have a background in electronic system design. In the future, this framework can be formalized into an end-to-end design tool that allows users to sketch, configure, and simulate designs in a single modeling environment to make the design process of MorphingCircuit more holistic.

9.5 Shape Limitation

In this paper, we only used the bending, twisting, and coiling deformation primitives, and the design space is limited to their combinations and their maximum twisting, coiling and bending angles. While MorphingCircuit can handle most of the developable shapes exemplified in this paper and other literature work [4, 63], non-developable shapes such as cones and saddles are not supported currently. In the future, we hope to improve our design tool by integrating non-developable shapes enabled by tools such as 4DMesh [62] and Geodesy [15] with conductive trace design and optimization, such that our method can yield design results with more complicated structures and less geometric constraints.

9.6 Fabrication Limitation

MorphingCircuit uses PLA as the substrate material, which can be deformed at a low temperature and handled with ease for the morphing process. However, this property also makes PLA incompatible with conventional reflow soldering methods. Therefore, MorphingCircuit is SMT-compatible while only supports limited (i.e., low-temperature) soldering methods. On the other hand, the 3D printed PLA substrates will shrink during the heat triggering process; even for the designed passive non-morphing part, it will have a ~6% shrinkage. If such a shrinkage phenomenon is carefully considered and compensated, it can be leveraged to fix the electronic components in place during the triggering. We designed two types of features - sinks and holes on the PLA substrates to hold two types of components - SMT and through-hole components. Since the size of these features are designed to be around 10% larger than the real size of the pins or components, components can be placed easily on the PLA substrates. After triggering, sinks and holes will shrink and hold the components tight.

Currently, our method can only print two layers of circuits on the substrate (front and back). In the future, multi-layer circuits and substrates can be combined to create circuits with higher complexity. Additionally, the oxidation of silver may affect the reliability of the circuit, therefore post-processing steps such as spraying insulation materials on the silver may be desired.

We use screen printing in our fabrication pipeline, and the resistivity of the silver ink is higher than traditional copper wire. This limits the use of high-power appliances and dissipates more heat than traditional PCB boards. In the future, we can explore conductive ink with lower resistivity or using copper tape with CNC cutting method to reduce power loss.

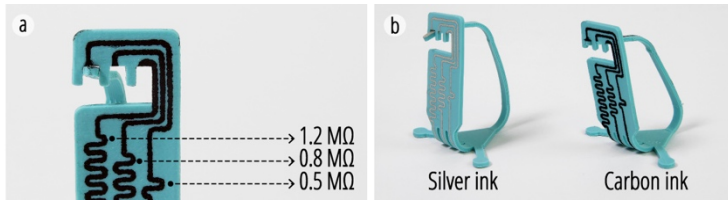


Fig. 18. Comparison of performances with silver ink and carbon ink.

9.7 Customized Tunable Components

We demonstrate three tunable components - resistors, capacitors and inductors with tunable values and the units of them are Ω , μF , and μH . The current value range of our tunable components is relatively small and can be improved by adjusting the structural design and changing our screen printing material. Taking the tunable resistor as an example, we print carbon-based conductive ink (MG chemicals-846) with the same structure of silver ink (Fig. 18) and discover the resistance value to be much larger ($0.5 \text{ M}\Omega$, $0.8 \text{ M}\Omega$ and $1.2 \text{ M}\Omega$). Notably, the carbon-based ink also has a different effect on the final shape of transformation due to its different mechanical properties. In the future, we could integrate more types of conductive inks in our FEA model to afford more design options.

9.8 Choice of Electrical Components

Due to the restriction in screen printing resolution, the minimum distance between pins should be 0.1 mm and minimum distance between components should be 0.7 mm. For SMD components, the minimum size we used is 1.6 mm by 0.8 mm; for through-hole components, the minimum diameter for the hole is 0.6 mm. Electrical components are assembled before triggering the PLA substrates, so they should be able to endure 90°C triggering temperature. For water triggering cases, batteries should be connected after triggering.

9.9 Material and Fabrication Tool Choices

When choosing conductive materials, we need to consider flexibility, conductivity, and curing temperature (if any). Other than the silver we used, we have explored different conductive material with various fabrication methods. We tried conductive carbon ink (Bare Conductive) with screen printing method but it's not flexible after curing. Using the same flexible silver ink, we tried the 3D printing method with an extrusion-based printer (Hyrel Engine SR, Hyrel 3D LLC) and was able to get 0.2 mm width of trace. However, the printing size is limited by the printing bed. We also tried using an inkjet printer (Chem3, LLC) to print silver, but the silver needed to be cured at around 80°C while printing. The success rate was low, and the temperature window at which the silver can be cured and the PLA is not triggered is too small. Besides printing, we also explored CNC-cut copper tape to make the connection, but it was hard to transform thin and flexible copper tape onto the PLA substrate while maintaining the shape. Overall, screen printing is, among the fast approaches, the easiest to operate.

10 CONCLUSIONS

In this paper, we present MorphingCircuit as a comprehensive design, simulation, and fabrication workflow to make 3D electronics. By leveraging the 4D printing technology, we envision a blooming future of “function integrated with form” in conformal electronics designs. With the interdisciplinary contribution, MorphingCircuit is not only a fast prototyping method for engineers and makers but also a platform for designers to integrate functionality into the form design. Through the fusion of aesthetics design and electronics, we intend to think beyond traditional 2D PCBs and incite a search for even larger design spaces of 4D printing technologies.

ACKNOWLEDGMENTS

This research was supported by the Carnegie Mellon University Manufacturing Futures Initiative, made possible by the Richard King Mellon Foundation; National Science Foundation grant IIS-2017008; and National Natural Science Foundation of China under Grant No. 62002321. The authors would also like to thank Danli Luo, Humphrey Yang, Lea Albaugh, Michael Rivera, Jianzhe Gu, Cathy Fang, Jack Forman, Koya Narumi, Huai-Yu Cheng, and Chengyuan Wei for their insights and support.

REFERENCES

- [1] *Voxel 8*. Available from: <https://www.voxel8.com/>.
- [2] J.J. Adams, E.B. Duoss, T.F. Malkowski, M.J. Motala, B.Y. Ahn, R.G. Nuzzo, J.T. Bernhard, J.A. Lewis 2011. Conformal printing of electrically small antennas on three-dimensional surfaces. *Advanced Materials* 23, 1335-1340.
- [3] B.Y. Ahn, E.B. Duoss, M.J. Motala, X. Guo, S.-I. Park, Y. Xiong, J. Yoon, R.G. Nuzzo, J.A. Rogers, J.A. Lewis 2009. Omnidirectional printing of flexible, stretchable, and spanning silver microelectrodes. *Science* 323, 1590-1593.
- [4] B. An, Y. Tao, J. Gu, T. Cheng, X.A. Chen, X. Zhang, W. Zhao, Y. Do, S. Takahashi, H.-Y. Wu, T. Zhang, L. Yao 2018. Thermorph: Democratizing 4D Printing of Self-Folding Materials and Interfaces. In *Proceedings of the 36th Annual ACM Conference on Human Factors in Computing Systems (CHI 2018)*, 260. DOI: <https://doi.org/10.1145/3173574.3173834>
- [5] M.D. Bartlett, N. Kazem, M.J. Powell-Palm, X. Huang, W. Sun, J.A. Malen, C. Majidi 2017. High thermal conductivity in soft elastomers with elongated liquid metal inclusions. *Proceedings of the National Academy of Sciences* 114, 2143-2148.
- [6] N. Bassik, G.M. Stern, D.H. Gracias 2009. Microassembly based on hands free origami with bidirectional curvature. *Applied physics letters* 95, 091901.
- [7] A.X. Chen, S. Coros, S.E. Hudson 2018. Medley: A Library of Embeddables to Explore Rich Material Properties for 3D Printed Objects. In *Proceedings of the 2018 CHI Conference on Human Factors in Computing Systems*, 162. DOI: <https://doi.org/10.1145/3173574.3173736>
- [8] C.-C. Chen, J.-Y. Chueh, H. Tseng, H.-M. Huang, S.-Y. Lee 2003. Preparation and characterization of biodegradable PLA polymeric blends. *Biomaterials* 24, 1167-1173.
- [9] I. Chtioui, F. Bossuyt, J. Vanfleteren, M.H. Bedouï 2018. 2.5/3D dynamically stretchable and permanently shaped electronic circuits. *Microsystem Technologies* 24, 831-853.
- [10] D. Espalin, D.W. Muse, E. MacDonald, R.B. Wicker 2014. 3D Printing multifunctionality: structures with electronics. *The International Journal of Advanced Manufacturing Technology* 72, 963-978.
- [11] S. Felton, M. Tolley, E. Demaine, D. Rus, R. Wood 2014. Applied origami. A method for building self-folding machines. *Science* 345, 644-646.
- [12] A.S. Gladman, E.A. Matsumoto, R.G. Nuzzo, L. Mahadevan, J.A. Lewis 2016. Biomimetic 4D printing. *Nature materials* 15, 413-418.
- [13] D. Groeger, J. Steimle 2019. LASEC: Instant Fabrication of Stretchable Circuits Using a Laser Cutter. In *Proceedings of the 2019 CHI Conference on Human Factors in Computing Systems*, 1-14. DOI: <https://doi.org/10.1145/3290605.3300929>
- [14] D. Groeger, J. Steimle 2018. ObjectSkin: augmenting everyday objects with hydroprinted touch sensors and displays. In *Proceedings of the ACM on Interactive, Mobile, Wearable Ubiquitous Technologies*, 1-23. DOI: <https://doi.org/10.1145/3161165>
- [15] J. Gu, D.E. Breen, J. Hu, L. Zhu, Y. Tao, T. Van de Zande, G. Wang, Y.J. Zhang, L. Yao 2019. Geodesy: Self-rising 2.5 D Tiles by Printing along 2D Geodesic Closed Path. In *Proceedings of the 2019 CHI Conference on Human Factors in Computing Systems*, 37. DOI: <https://doi.org/10.1145/3290605.3300267>
- [16] G.J. Hayes, Y. Liu, J. Genzer, G. Lazzi, M.D. Dickey 2014. Self-folding origami microstrip antennas. *IEEE Transactions on Antennas Propagation* 62, 5416-5419.
- [17] S. Hodges, N. Villar, N. Chen, T. Chugh, J. Qi, D. Nowacka, Y. Kawahara 2014. Circuit stickers: peel-and-stick construction of interactive electronic prototypes. In *Proceedings of the SIGCHI Conference on Human Factors in Computing Systems*, 1743-1746. DOI: <https://doi.org/10.1145/2556288.2557150>
- [18] F. Hu, L. Lyu, Y. He 2019. A 3D Printed Paper-Based Thermally Driven Soft Robotic Gripper Inspired by Cabbage. *International Journal of Precision Engineering Manufacturing* 20, 1915-1928.
- [19] Y. Huang, H. Wu, L. Xiao, Y. Duan, H. Zhu, J. Bian, D. Ye, Z. Yin 2019. Assembly and applications of 3D conformal electronics on curvilinear surfaces. *Materials Horizons* 6, 642-683.
- [20] S.E. Hudson 2014. Printing teddy bears: a technique for 3D printing of soft interactive objects. In *Proceedings of the CHI 2014*, 459-468. DOI: <https://doi.org/10.1145/2556288.2557338>
- [21] R.J. Jackman, J.L. Wilbur, G.M. Whitesides 1995. Fabrication of submicrometer features on curved substrates by microcontact printing. *Science* 269, 664-666.
- [22] S. Janbaz, R. Hedayati, A. Zadpoor 2016. Programming the shape-shifting of flat soft matter: from self-rolling/self-twisting materials to self-folding origami. *Materials Horizons* 3, 536-547.
- [23] M. Jobs, K. Hjort, A. Rydberg, Z. Wu 2013. A tunable spherical cap microfluidic electrically small antenna. *Small* 9, 3230-3234.
- [24] H.-L. Kao, A. Dementyev, J.A. Paradiso, C. Schmandt 2015. NailO: fingernails as an input surface. In *Proceedings of the 33rd Annual ACM Conference on Human Factors in Computing Systems*, 3015-3018. DOI: <https://doi.org/10.1145/2702123.2702572>
- [25] Y. Kawahara, S. Hodges, B.S. Cook, C. Zhang, G.D. Abowd 2013. Instant inkjet circuits: lab-based inkjet printing to support rapid prototyping of UbiComp devices. In *Proceedings of the 2013 ACM international joint conference on Pervasive and ubiquitous computing*, 363-372. DOI: <https://doi.org/10.1145/2493432.2493486>

- [26] A. Khan, J.S. Roo, T. Kraus, J. Steimle 2019. Soft Inkjet Circuits: Rapid Multi-Material Fabrication of Soft Circuits Using a Commodity Inkjet Printer. In *Proceedings of the 32nd Annual ACM Symposium on User Interface Software and Technology*, 341-354. DOI: <https://doi.org/10.1145/3332165.3347892>
- [27] G. Laput, E. Brockmeyer, S.E. Hudson, C. Harrison 2015. Acoustuments: Passive, acoustically-driven, interactive controls for handheld devices. In *Proceedings of the 33rd Annual ACM Conference on Human Factors in Computing Systems*, 2161-2170. DOI: <https://doi.org/10.1145/2782782.2792490>
- [28] B. Le Borgne, O. De Sagazan, S. Crand, E. Jacques, M. Harnois 2017. Conformal electronics wrapped around daily life objects using an original method: water transfer printing. *ACS applied materials interfaces* 9, 29424-29429.
- [29] R.-H. Liang, H.-C. Kuo, L. Chan, D.-N. Yang, B.-Y. Chen 2014. GaussStones: shielded magnetic tangibles for multi-token interactions on portable displays. In *Proceedings of the 27th annual ACM symposium on User interface software and technology*, 365-372. DOI: <https://doi.org/10.1145/2642918.2647384>
- [30] J. Lo, E. Paulos 2014. ShrinkyCircuits: sketching, shrinking, and formgiving for electronic circuits. In *Proceedings of the 27th annual ACM symposium on User interface software and technology*, 291-299. DOI: <https://doi.org/10.1145/2642918.2647421>
- [31] J. Lo, C. Torres, I. Yang, J. O'Leary, D. Kaufman, W. Li, M. Dontcheva, E. Paulos 2016. Aesthetic electronics: Designing, sketching, and fabricating circuits through digital exploration. In *Proceedings of the 29th Annual Symposium on User Interface Software and Technology*, 665-676. DOI: <https://doi.org/10.1145/2984511.2984579>
- [32] Y. Mao, Z. Ding, C. Yuan, S. Ai, M. Isakov, J. Wu, T. Wang, M.L. Dunn, H.J. Qi 2016. 3D printed reversible shape changing components with stimuli responsive materials. *Scientific reports* 6, 1-13.
- [33] E. Markvicka, G. Wang, Y.-C. Lee, G. Laput, C. Majidi, L. Yao 2019. ElectroDermis: Fully Untethered, Stretchable, and Highly-Customizable Electronic Bandages. In *Proceedings of the 2019 CHI Conference on Human Factors in Computing Systems*, 632. DOI: <https://doi.org/10.1145/3290605.3300862>
- [34] S. Miyashita, L. Meeker, M.T. Tolley, R.J. Wood, D. Rus 2014. Self-folding miniature elastic electric devices. *Smart Materials and Structures* 23, 094005.
- [35] F. Momeni, X. Liu, J. Ni 2017. A review of 4D printing. *Materials & Design* 122, 42-79.
- [36] F. Momeni, S. Sabzpushan, R. Valizadeh, M.R. Morad, X. Liu, J. Ni 2019. Plant leaf-mimetic smart wind turbine blades by 4D printing. *Renewable Energy* 130, 329-351.
- [37] N. Münnzenrieder, G. Cantarella, C. Vogt, L. Petti, L. Büthe, G.A. Salvatore, Y. Fang, R. Andri, Y. Lam, R. Libanori 2015. Stretchable Electronics: Stretchable and Conformable Oxide Thin-Film Electronics (Adv. Electron. Mater. 3/2015). *Advanced Electronic Materials* 1.
- [38] S. Olberding, S. Soto Ortega, K. Hildebrandt, J. Steimle 2015. Foldio: Digital fabrication of interactive and shape-changing objects with foldable printed electronics. In *Proceedings of the UIST 2015*, 223-232. DOI: <https://doi.org/10.1145/2807442.2807494>
- [39] S. Olberding, M. Wessely, J. Steimle 2014. Printscreen: fabricating highly customizable thin-film touch-displays. In *Proceedings of the UIST 2014*, 281-290. DOI: <https://doi.org/10.1145/2642918.2647413>
- [40] J.A. Paulsen, M. Renn, K. Christenson, R. Plourde 2012. Printing conformal electronics on 3D structures with Aerosol Jet technology. In *Proceedings of the 2012 Future of Instrumentation International Workshop (FIIW) Proceedings*, 1-4. DOI: <https://doi.org/10.1145/3313831.3376543>
- [41] H. Peng, J. Mankoff, S.E. Hudson, J. McCann 2015. A layered fabric 3D printer for soft interactive objects. In *Proceedings of the CHI 2015*, 1789-1798. DOI: <https://doi.org/10.1145/2702123.2702327>
- [42] B. Plovie, Y. Yang, J. Guillaume, S. Dunphy, K. Dhaenens, S. Van Put, B. Vandecasteele, T. Vervust, F. Bossuyt, J. Vanfleteren 2017. Arbitrarily shaped 2.5 d circuits using stretchable interconnects embedded in thermoplastic polymers. *Advanced Engineering Materials* 19, 1700032.
- [43] B. Plovie, Y. Yang, J. Guillaume, S. Dunphy, K. Dhaenens, S. Van Put, T. Vervust, F. Bossuyt, J. Vanfleteren 2016. One-time deformable thermoplastic devices based on flexible circuit board technology. In *Proceedings of the 2016 11th International Microsystems, Packaging, Assembly and Circuits Technology Conference (IMPACT)*, 125-128.
- [44] J. Qi, L. Buechley 2014. Sketching in circuits: designing and building electronics on paper. In *Proceedings of the SIGCHI Conference on Human Factors in Computing Systems*, 1713-1722. DOI: <https://doi.org/10.1145/2556288.2557391>
- [45] J.N. Reddy 2006. *Theory and analysis of elastic plates and shells*. CRC press.
- [46] G. Saada, M. Layani, A. Chernevousky, S. Magdassi 2017. Hydroprinting conductive patterns onto 3D structures. *Advanced Materials Technologies* 2, 1600289.
- [47] V. Savage, C. Chang, B. Hartmann 2013. Sauron: embedded single-camera sensing of printed physical user interfaces. In *Proceedings of the 26th annual ACM symposium on User interface software and technology*, 447-456. DOI: <https://doi.org/10.1145/2501988.2501992>
- [48] V. Savage, S. Follmer, J. Li, B. Hartmann 2015. Makers' Marks: Physical markup for designing and fabricating functional objects. In *Proceedings of the 28th Annual ACM Symposium on User Interface Software & Technology*, 103-108. DOI: <https://doi.org/10.1145/2807442.2807508>
- [49] M. Schmitz, M. Khalilbeigi, M. Balwierz, R. Lissermann, M. Mühlhäuser, J. Steimle 2015. Capriate: A fabrication pipeline to design and 3D print capacitive touch sensors for interactive objects. In *Proceedings of the 28th Annual ACM Symposium on User Interface Software & Technology*, 253-258. DOI: <https://doi.org/10.1145/2807442.2807503>
- [50] M. Schmitz, J. Steimle, J. Huber, N. Dezfuli, M. Mühlhäuser 2017. Flexibles: deformation-aware 3D-printed tangibles for capacitive touchscreens. In *Proceedings of the 2017 CHI Conference on Human Factors in Computing Systems*, 1001-1014. DOI: <https://doi.org/10.1145/3025453.3025663>
- [51] H. Sun, Z. Han, N. Willenbacher 2019. Ultrastretchable conductive elastomers with a low percolation threshold for printed soft electronics. *ACS applied materials interfaces* 11, 38092-38102.

- [52] L. Sun, J. Li, Y. Chen, Y. Yang, Y. Tao, G. Wang, L. Yao 2020. 4DTexture: A Shape-Changing Fabrication Method for 3D Surfaces with Texture. In *Proceedings of the Extended Abstracts of the 2020 CHI Conference on Human Factors in Computing Systems*, 1-7. DOI: <https://doi.org/10.1145/3334480.3383053>
- [53] L. Sun, Y. Yang, Y. Chen, J. Li, G. Wang, Y. Tao, L. Yao 2020. ShrinkyKit: 3D Printing Shrinkable Adaptations for Everyday Objects. In *Proceedings of the Extended Abstracts of the 2020 CHI Conference on Human Factors in Computing Systems*, 1-7. DOI: <https://doi.org/10.1145/3334480.3383034>
- [54] S. Sundaram, D.S. Kim, M.A. Baldo, R.C. Hayward, W. Matusik 2017. 3D-printed self-folding electronics. *ACS applied materials interfaces* 9, 32290-32298.
- [55] S. Swaminathan, K.B. Ozutemiz, C. Majidi, S.E. Hudson 2019. FiberWire: Embedding Electronic Function into 3D Printed Mechanically Strong, Lightweight Carbon Fiber Composite Objects. In *Proceedings of the 2019 CHI Conference on Human Factors in Computing Systems*, 1-11. DOI: <https://doi.org/10.1145/3290605.3300797>
- [56] Y. Tao, Y. Do, H. Yang, Y.-C. Lee, G. Wang, C. Mendoza, J. Cui, W. Wang, L. Yao 2019. Morphlour: Personalized Flour-based Morphing Food Induced by Dehydration or Hydration Method. In *Proceedings of the 32nd Annual ACM Symposium on User Interface Software and Technology*, 329–340. DOI: [10.1145/3332165.3347949](https://doi.org/10.1145/3332165.3347949)
- [57] E. Tenckhoff 1988. *Deformation mechanisms, texture, and anisotropy in zirconium and zircaloy*. ASTM International.
- [58] S. Tibbits 2014. 4D printing: multi-material shape change. *Architectural Design* 84, 116-121.
- [59] T. van Manen, S. Jambaz, A.A. Zadpoor 2017. Programming 2D/3D shape-shifting with hobbyist 3D printers. *Materials Horizons* 4, 1064-1069.
- [60] T. Vasilevitsky, A. Zoran 2016. Steel-sense: Integrating machine elements with sensors by additive manufacturing. In *Proceedings of the 2016 CHI Conference on Human Factors in Computing Systems*, 5731-5742. DOI: <https://doi.org/10.1145/2858036.2858309>
- [61] G. Wang, T. Cheng, Y. Do, H. Yang, Y. Tao, J. Gu, B. An, L. Yao 2018. Printed Paper Actuator: A Low-cost Reversible Actuation and Sensing Method for Shape Changing Interfaces. In *Proceedings of the 2018 CHI Conference on Human Factors in Computing Systems*, 569. DOI: <https://doi.org/10.1145/3173574.3174143>
- [62] G. Wang, Y. Humphrey, Z. Yan, N.G. Ulu, Y. Tao, J. Gu, L.B. Kara, L. Yao 2018. 4DMesh: 4D Printing Self-Folding Non-Developable Mesh Surfaces. In *Proceedings of the 2018 ACM Symposium on User Interface Software and Technology (UIST'18)*. DOI: <https://doi.org/10.1145/3242587.3242625>
- [63] G. Wang, Y. Tao, O.B. Capunaman, H. Yang, L. Yao 2019. A-line: 4D Printing Morphing Linear Composite Structures. In *Proceedings of the 37th Annual ACM Conference on Human Factors in Computing Systems (CHI 2019)*, 426. DOI: <https://doi.org/10.1145/3290605.3300656>
- [64] W. Wang, L. Yao, T. Zhang, C.-Y. Cheng, D. Levine, H. Ishii 2017. Transformative Appetite: Shape-Changing Food Transforms from 2D to 3D by Water Interaction through Cooking. In *Proceedings of the CHI 2017*, 6123-6132. DOI: <https://doi.org/10.1145/3025453.3026019>
- [65] J.P. Whitney, P.S. Sreetharan, K.Y. Ma, R.J. Wood 2011. Pop-up book MEMS. *Journal of Micromechanics and Microengineering* 21.
- [66] D. Wigdor 2015. Printem: Instant Printed Circuit Boards with Standard Office Printers & Inks. In *Proceedings of the 28th Annual ACM Symposium on User Interface Software & Technology*, 243-251. DOI: <https://doi.org/10.1145/2807442.2807511>
- [67] K. Willis, E. Brockmeyer, S. Hudson, I. Poupyrev 2012. Printed optics: 3D printing of embedded optical elements for interactive devices. In *Proceedings of the 25th annual ACM symposium on User interface software and technology*, 589-598. DOI: <https://doi.org/10.1145/2380116.2380190>
- [68] J. Wu, C. Yuan, Z. Ding, M. Isakov, Y. Mao, T. Wang, M.L. Dunn, H.J. Qi 2016. Multi-shape active composites by 3D printing of digital shape memory polymers. *Scientific reports* 6, 24224.
- [69] J. Yamaoka, M.D. Dogan, K. Bulovic, K. Saito, Y. Kawahara, Y. Kakehi, S. Mueller 2019. FoldTronics: Creating 3D Objects with Integrated Electronics Using Foldable Honeycomb Structures. In *Proceedings of the 2019 CHI Conference on Human Factors in Computing Systems*, 1-14. DOI: <https://doi.org/10.1145/3290605.3300858>
- [70] J. Yamaoka, Y. Kakehi 2017. ProtoMold: An interactive vacuum forming system for rapid prototyping. In *Proceedings of the 2017 CHI Conference on Human Factors in Computing Systems*, 2106-2115. DOI: <https://doi.org/10.1145/3025453.3025498>
- [71] S. Yoon, K. Choi, S. Baek, H. Chang 2011. Electronic circuit patterning on curved surface by direct laser structuring. In *Proceedings of the 2011 International Conference on Electrical Machines and Systems*, 1-3. DOI: [10.1109/ICEMS.2011.6073785](https://doi.org/10.1109/ICEMS.2011.6073785)
- [72] Y. Yu, H. Liu, K. Qian, H. Yang, M. McGehee, J. Gu, D. Luo, L. Yao, Y.J. Zhang 2020. Material characterization and precise finite element analysis of fiber reinforced thermoplastic composites for 4D printing. *Computer-Aided Design* 122, 102817.
- [73] C. Zheng, H. Oh, L. Devendorf, E.Y.-L. Do 2019. Sensing kirigami. In *Proceedings of the 2019 on Designing Interactive Systems Conference*, 921-934. DOI: <https://doi.org/10.1145/3322276.3323689>
- [74] J. Zhu, L.-G. Blumberg, Y. Zhu, M. Nisser, E.L. Carlson, X. Wen, K. Shum, J.A. Quaye, S. Mueller 2020. CurveBoards: Integrating Breadboards into Physical Objects to Prototype Function in the Context of Form. In *Proceedings of the 2020 CHI Conference on Human Factors in Computing Systems*, 1-13. DOI: <https://doi.org/10.1145/3313831.3376617>